UNIVERSITY of CALIFORNIA
Santa Barbara

Cellular Topological Packings in Early Embryos

A dissertation submitted in partial satisfaction of the
requirements for the degree of

Doctor of Philosophy

in

Physics

by

James Giammona

Committee in charge:

Professor Otger Campàs, Co-Chair

Professor Philip A. Pincus, Co-Chair

Professor Jean Carlson

March 2020

The dissertation of James Giammona is approved:

Professor Jean Carlson

Professor Philip A. Pincus, Co-Chair

Professor Otger Campàs, Co-Chair

January 2020

To my parents, William, and Bethany, thank you for your unwavering love and support.

Acknowledgements

First, I'd like to extend my sincerest thanks and gratitude to my advisor, Otger Campàs. I would not have been able to finish this work without his years of guidance, encouragement, collaboration, and friendship. I've learned so much about how to conduct excellent theoretical and computational research and these perspectives and skills will be valuable for the rest of my life, especially how to find the important scales and dimensionless parameters of any problem. I've been lucky to have seen several of the lab's projects go from an exploratory beginning, through the years of confusing data and the eventual understanding to the final polished paper and enjoyed seeing how Otger approached each stage of research. Such first-hand experience has been the most valuable part of my PhD.

Next, I'd like to recognize the invaluable assistance of my committee members: Jean Carlson and Fyl Pincus. Their expertise, encouragement, and advice helped me at many points throughout this journey and they both always brightened my day when our paths crossed walking around campus. In addition, working with Professor Carlson on Physics Circus for three years was one of the highlights of graduate school. I'm so glad to have had the opportunity to bring such joy with hands-on demonstrations to so many kids and parents.

I will always be indebted to everyone in the Campàs lab past and present for their help and friendship. Thank you to Samhita, Elijah, Payam, Georgina, Carlos, Sangwoo, Marie, Antoine, Yucen, Ben, Jamie, Mishel, David, Hannah, Alessandro, Friedhelm, and Renwei for making every day fun and interesting! I've learned a lot from all of you and couldn't have asked for better colleagues.

Thank you to everyone in the Physics department who's helped me in many ways large and small. I'd like to offer special thanks to Jennifer Farrar who has helped me so many times throughout my PhD. I'd also like to recognize all my fellow graduate student friends. I couldn't have made it through classes and research without your help, friendship, and support. I'll fondly remember late nights together in the Broida trailer.

Finally, thank you to all my wonderful friends and loving family. Your constant encouragement and support was invaluable. Thank you William for years of good conversations. Thank you Mom and Dad for a lifetime of love and support. Thank you Bethany for always being there for me. I couldn't have done it without you!

Curriculum Vitæ

James Giammona

Education

2020 Ph.D., Physics, University of California, Santa Barbara

2013 B.S., Physics, Yale University, New Haven

Professional Experience

2013-2019 Graduate Teaching Assistant, University of California, Santa Barbara

2019-2020 Graduate Student Researcher, University of California, Santa Barbara

Publications

Mongera, A., Rowghanian, P., Gustafson, H. J., Shelton, E., Kealhofer, D. A., Carn, E. K., et al. (2018). A fluid-to-solid jamming transition underlies vertebrate body axis elongation. *Nature*, 561(7723), 401-405.

Giammona, J., Campàs, O. (in prep.) Blastomere packings under confinement.

Giammona, J., Campàs, O. (in prep.) Robustness of the *C. elegans* early embryo cellular arrangements to noise.

Outreach and Mentoring

2016-2019 Physics Circus Coordinator, University of California, Santa Barbara

2019 Graduate Student Mentor, University of California, Santa Barbara

Abstract

Cellular Topological Packings in Early Embryos

by

James Giammona

At very early embryonic stages, when embryos are composed of just a few cells, establishing the correct packing arrangements (contacts) between cells is essential for proper development of the organism. As early as the 4-cell stage, the observed blastomere packings in different species are different and, in many cases, differ from the equilibrium packings expected for simple adherent and deformable particles.

We use a novel 3D Voronoi-augnemted Langevin simulator to systematically study how the forces between blastomeres, their division rates, orientation of cell division, and embryonic confinement influence the final packing configurations. In the absence of physical confinement of the embryo, we find that blastomere packings are not robust, with multiple packing configurations simultaneously possible (degeneracy) and are very sensitive to parameter changes. Our results indicate that the geometry of the embryonic confining shell determines the packing configurations at the 4-cell stage, removing degeneracy in the possible packing configurations and overriding division rules in most cases.

Furthermore, we use our simulator to study the robustness of the *C. elegans* early

embryo to noise in division timing and angle. We find that there exists a range of timing and angular noise that the embryo is fully robust to and categorize the errors outside this regime as coming from mistimed divisions or misplaced cells. We also study how robust the embryo is to overall shifts in the timing offset between the AB and P1 divisions and find that even large changes can be non-lethal. Finally, we systematically investigate how robust the embryo is to deterministic shifts in division directions from the wildtype rules and find that the major source of lethal error is from offsets of more than 90 degrees to the P2-EMS division axis. Overall, our results demonstrate how confinement, division timing and division rules all contribute to ensuring robust development with confinement setting the overall packing topology and division timings and rules specifying where individual cells will go within that shape.

Contents

Chapter 1

Introduction

1.1 Blastomere arrangements in early development

The intricately complex pattern of morphogenesis that leads to a developed multicellular organism begins with a single fertilized egg cell. For species where the egg's subsequent division is holoblastic (the entire cell divides fully in two)[19], the first few divisions and the resulting cellular positions at the 4 to 8 cell stages are often critical for correct further development. Cell-cell signalling occurs through surface contact between neighboring cells and the early embryo's cellular arrangement set the topology of contacts between cells. This cell-cell signalling provides necessary information that leads to subsequent cell fate determination. The fates assigned to these early cells set the body plan of the organism determining the anterior-posterior axis , dorsal-ventral axis, left-right axis and the stem cell progenitors of the organism's tissues and organs[30, 47, 19]. Errors in the arrangements of cells in the early embryo can lead to drastic developmental changes (like

reversal of left-right handedness[70, 59]) and can often be lethal.

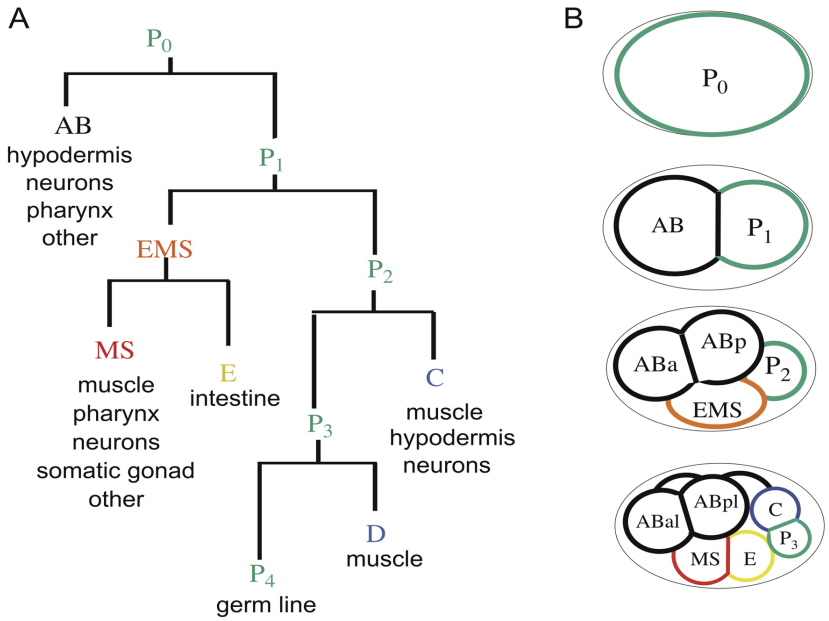

Figure 1.1: **Generation of founder cells in the early *C. elegans* embryo.** Anterior is to the left, posterior to the right, dorsal is up and ventral down in this and all subsequent figures. A: Cell lineage of the early embryo. The horizontal lines connect sister cells; the length of the vertical lines indicates the relative cell cycle duration of each founder cell. The major cell types produced from each founder cell are shown. B: Schematic diagram of cell positions at different stages. The germ-line precursors (P cells) are shown outlined with green, and each of the founder cells generated by asymmetric division are indicated with a different color. The daughters of founder cells are named by their position; e.g., ABa is the anterior daughter of AB, whereas ABal is the left daughter of ABa. The embryo proper is surrounded by an eggshell, schematized by a black line. Reproduced from [30] under a CC-A license

A representative and well-studied example of the importance of early cell positioning for proper subsequent development is the nematode worm, *C. elegans*, which has a highly conserved and stereotypical pattern of cell arrangements throughout development[62]. Already after the first division of the egg, the anterior-posterior axis is established due to an asymmetric division caused in part by different PAR polarity proteins being expressed in the two sides of the egg[30] leading to an anterior blastomere (called AB) and a smaller posterior blastomere (called P1). After the second round of divisions, the arrangements

and contacts between the four cells is crucial to set the proper cell lineages during later development.

The AB blastomere divides perpendicularly to the anterior-posterior axis and the two daughter cells are then skewed by the confinement of the hard chitinous eggshell that surrounds the embryo[30, 54]. The more anterior daughter is designated ABa and the more posterior daughter is referred to as ABp. In wildtype development, only descendents of the ABa blastomere produce pharyngeal muscle cells and not descendents of the ABp blastomere[48]. However, experimentally interchanging ABa and ABp still leads to normal development and is strong evidence that ABa and ABp are initially equivalent. It is contact between ABp and the P1 daughter P2 that causes the change ABp's fate specification.

A few minutes after the AB division, P1 divides unequally along the anterior-posterior axis into the larger EMS and smaller P2 daughter cells. The position of the EMS cell defines the ventral side of the embryo and its contact with P2 leads EMS to asymmetrically divide with the larger anterior MS becoming a major muscle precursor while the smaller posterior E cell becomes the precursor of all intestinal tissue. Already, at this early stage, two different cell-cell signalling pathways are used to guide the fates of those cells in contact with P2, with the Wnt pathway specifying the subsequent EMS development and the Notch/Delta pathway changing the fate of ABp, both of which are highly conserved throughout the animal kingdom[68, 12, 4, 30].

The fate divergence between ABa and ABp is induced by the Notch/Delta signalling

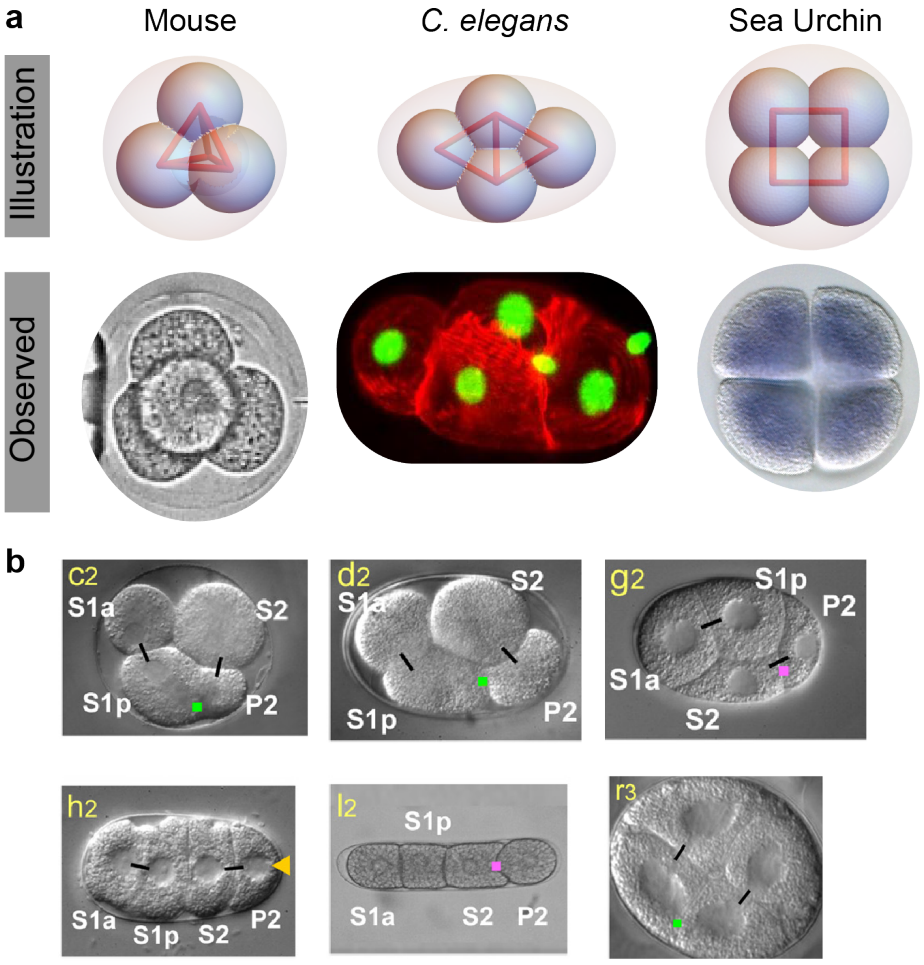

Figure 1.2: **Diversity of 4-cell embryo arrangements** A: Illustration and microscope observations of the tetrahedral mouse embryo (image from [18]), the diamond arrangement of *C. elegans* (image from [17]), and the square sea urchin embryo (image from [24]). B: Six distinct nematode species at the 4-cell stage showing many different cell packings and shell aspect ratios (from [57]).

pathway[49]. Both ABa and ABp express the Notch transmembrane receptor, but only P2 expresses the Delta ligand. Because of the positioning of P2 in the posterior of the embryo, only ABp comes into contact with P2 and has its gene expression modified. Interchanging the positions of EMS and P2 (causing both ABa and ABp to contact P2's Delta ligands) leads to major abnormalities while interchange of ABa and ABp leads to

the same pattern where only one of the two AB daughters gets the signal from P2[48].

While the proper early embryo arrangement is important for any given species, there is significant variation in the arrangement patterns between species. For example, at the 4-cell stage, mouse embryos (and many other mammals) form a tetrahedron[46, 18, 23], echinoderms form a square[19, 37], the nematode worm C. elegans forms a diamond[30], and other nematode species form linear arrangements as well as the previous arrangements mentioned[57, 21] (see Figure 1.2). How do different species robustly control their cellular arrangements at this early stage?

1.2 Physical interactions between cells and cell division rules

Physical interactions between cells mainly arise from cortical tension and cell-cell adhesion. Animal cells contain an active acto-myosin matrix about 50-100 nm thick below the plasma membrane which provides much of the cell's mechanical properties[53]. On timescales shorter than the time for actin turnover (< 1 min), the cortex behaves as an elastic solid[53]. The cortex also experiences myosin driven contractility which resists the cell's internal osmotic pressure and generates the cell's cortical tension which can vary from 10s to 1000s of piconewtons per micron[32, 53, 61].

Cells adhere to each other mainly through transmembrane proteins called cadherins which anchor to the acto-myosin cortex and bind with analogous cadherins expressed on

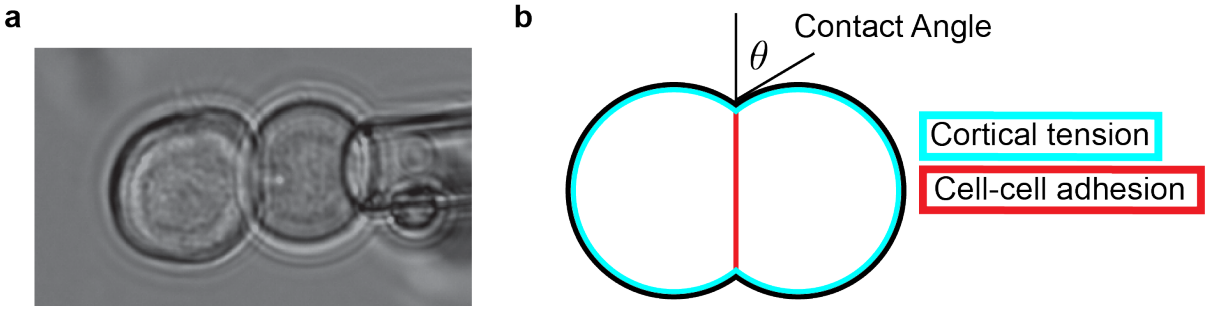

Figure 1.3: **Cortical tension and adhesion between cells lead to contact angle** A: Embryonic zebrafish endoderm doublet (with micropipette on right). From [34]. B: Schematic illustrating the actomyosin cortex (cyan) which generates cortical tension through myosin contractility and adhesion between cell surfaces (red) mediated primarily by cadherins.

neighboring cell surfaces[6]. Adhesion usually results in a lowering of surface energy per area or interfacial tension for the regions in contact which can be measured by observing the junction's contact angle or by micropipette aspiration[35]. The overall shape and amount of contact area between cells results from an interplay between cortical tension and cell-cell adhesion.

Cells divide and the direction of their division is specified by an interplay between cell shape, cell polarity and other biochemical cues[41, 40, 45, 20]. The cleavage plane is set by the orientation and position of the mitotic spindle which is usually positioned by forces applied by microtubules extending from the centromeres. As was previously mentioned, proper cell positioning is integral to proper development and one of the main determinants of cell position is division plane positioning. In early holoblastic embryos, cell divisions are volume conserving, but are sometimes asymmetric with one daughter larger than the other.

Given that cells can exert active forces (including when dividing) and given damping effects due to the cortex acting as a viscous fluid on timescales longer than a minute which

lead to a characteristic time to relax stresses[53], cell clusters can be out-of-equilibrium. Cell divisions can place cells in arrangements that are not the lowest energy equilibrium arrangement and can even divide again before fully relaxing leading to a trajectory of non-equilibrium configurations. To understand what cell packings are possible from division rules, it is necessary to use non-equilibrium methods.

1.3 Equilibrium arrangements of small sphere clusters

Perhaps the cellular arrangements observed in different species' early development are the natural equilibrium configurations for four cells and embryos are passively guided by energetic and entropic considerations to their observed packings? The minimal energy configurations of small clusters of hard spheres has only recently been systematically studied. In 1995, Sloane *et al.*[60] numerically and algorithmically searched for the tightest packings of N (< 32) equal non-overlapping spheres that minimized the second-moment about the cluster's centroid. For the N=4 case, they find that the tetrahedron is the tightest packing and propose putative optimal clusters up to N=32. Intriguingly, such clusters were observed experimentally. Manoharan *et al.*[36] found that polystyrene microspheres contained in slowly evaporating toluene droplets ended up in clusters that minimized their second-moment.

Other packings are favored for clusters of hard spheres with short-range attractions.

In this case, the energy of a cluster is fully specified by the number of contacts between spheres. Natalie Arkus and colleagues[2, 3] used adjacency matrices, graph isomorphism and geometric rules to determine the minimal energy clusters for short-ranged interactions. For N cells, the pattern of contacts between pairs of spheres can be represented by an N by N symmetric matrix called an adjacency matrix $\mathcal{A}$ where the existence of contact between sphere i and sphere j is denoted by setting the $\mathcal{A}_{ij}$ and $\mathcal{A}_{ji}$ values to 1. Graph isomorphism algorithms were used to determine if two different adjacency matrices represented the same underlying graph of connections with permuted labels of spheres. The subset of topologically distinct adjacency matrices were then filtered by using geometrically motivated rules to determine if an adjacency matrix was impossible to realize physically due to sphere intersections and rigidity constraints (cells must have at least 3 contacts to be held rigidly in place and the cluster must have a total of at least 3n-6 total contacts).

Arkus *et al.*[2, 3] enumerated all topologically distinct minimal energy rigid clusters up to N=20 and their list included all previously observed and theorized minimal second-moment clusters plus newly described clusters. At N=4, the tetrahedron is again the only minimal cluster, but beginning with N=6, two clusters with the same contact energy appear. The degeneracy increases to 6 for clusters with seven spheres and 16 for clusters with eight. Are all these clusters equally likely to appear in experiments with clusters of hard spheres with short-ranged attraction if they all have the same energy?

Surprisingly, the clusters are not observed to form with equal frequencies. Meng *et*

al.[38] placed polystyrene microspheres in a small cylindrical well filled with a solution with much smaller polyNIPAM nanoparticles that created an effective short-ranged depletion interaction between the microspheres and observed the frequency of clusters that were present in the wells after they had reached equilibrium. In the six sphere cluster for example, the less symmetric polytetrahedron cluster is observed 80% of the time while the more symmetric octahedron which is only observed 5% of the time. Meng *et al.* explained this observation by calculating the rotational and vibrational entropy difference between the two clusters and used this to determine the free energies of each cluster. The observations were found to mostly match the probabilities predicted by the theoretical free energy values. Those clusters with less symmetry had more rotational entropy and therefore more free energy. These observations lead to the conclusion that free energy of a cluster and not purely its energy is the right quantity to compare and predict the occurrence of small sphere clusters.

However, for four spheres, all the above methods only found one minimal energy cluster, the tetrahedron, and so only the tetrahedron is expected to be observed in equilibrium. How then are early embryos creating and maintaining arrangements other than the tetrahedron? Are these cell clusters out of equilibrium or are there extra physical constraints that are influencing the cluster arrangement? Numerical simulation presents a method to test these hypotheses.

1.4 Previous models of cellular packings in early development

Two main approaches are used to model the arrangements of cells in the early embryo: non-equilibrium particle-based models which have no shape information and models that calculate detailed equilibrium cell shapes coupled with a shape-based division plane model. It's important to note that particle-based approaches can model non-equilibrium packings which have not yet relaxed to equilibrium because they explicitly model the dynamics of the cluster, while the shape-based model only transitions between equilibrium states and does not simulate dynamics.

The model used by Fickentscher *et al.* (2013)[15] exemplifies the non-equilibrium particle approach which was used to study the early development of *C. elegans*. Fickentscher *et al.* chose to represent the blastomeres in the early embryo as soft spheres and used a minimal particle-based model where each cell center interacted with other cell centers and an ellipsoid representing the external eggshell via a quadratic repulsive potential (Fig 1.4a). The model was only used to simulate the trajectories of blastomeres between divisions so the division times and division direction for each cell was imposed by hand. Total cell volume was conserved among all cells and fixed to be equal to the shell volume. Cell trajectories were obtained by numerically integrating a model of overdamped Langevin dynamics for each cell and were compared to those from real embryos obtained by selective plane illumination microscopy (SPIM).

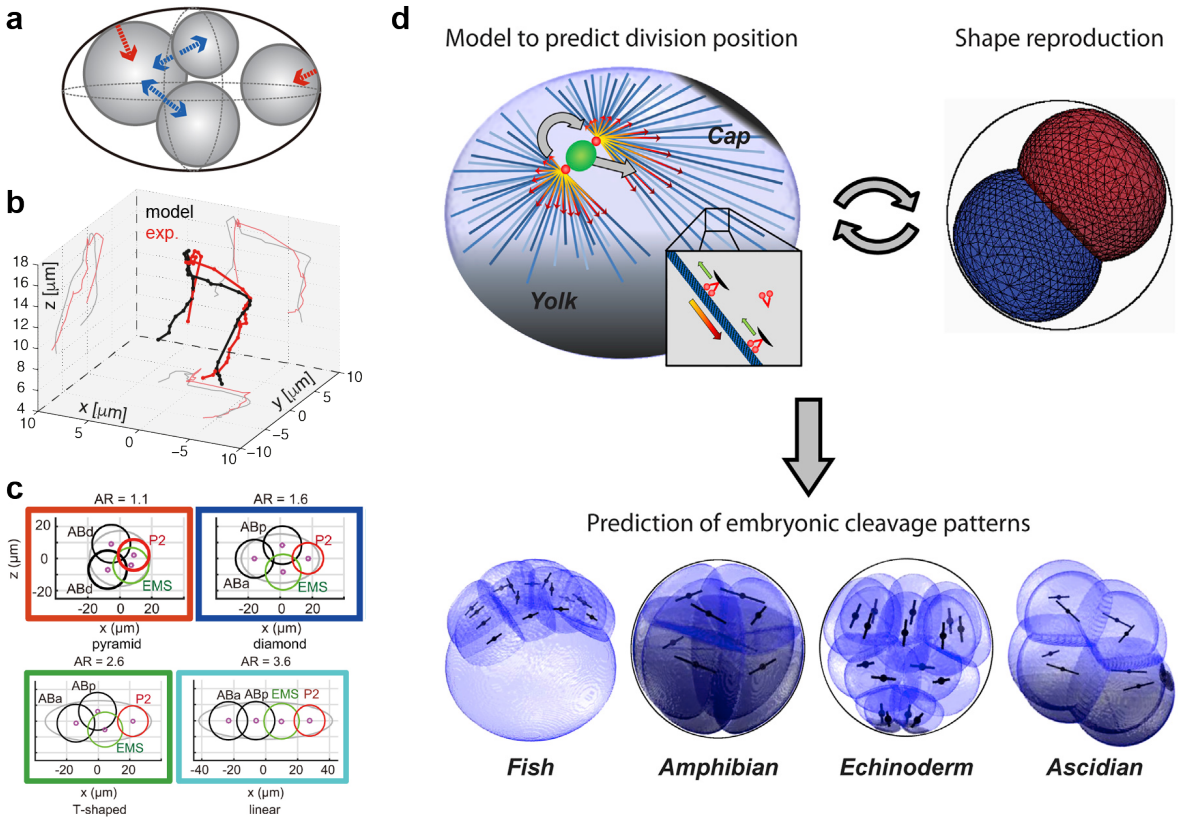

Figure 1.4: **Particle-based and shape-based simulations** A: Illustration of the particle-based model used by Fickentscher[15] with cell-cell (blue) and cell-shell (red) forces. (Image from [72].) B: Figure demonstrating the particle trajectories closely follow those observed in experiment. (Image from [15]) C: Yamamoto and Kimura adapted the model to study how changing the shell aspect ratio affected the cell arrangements. Here pyramid, diamond, T-shaped, and linear arrangements are found. (Image from [72]) D: Pierre *et al.*[45] used a combination of a shape based model for divsision plane positioning coupled to the energy minimizing Surface Evolver[10] to generate qualitatively similar embryos to those observed for fish, amphibians, echinoderms, and ascidians. (Image from [45])

The trajectories of cell motion between divisions was remarkably conserved between live embryos and were also well matched by Fickentscher *et al.*'s minimal model up to the 12-cell stage (Fig 1.4b). They also noted that the cells reproduced the planar diamond arrangement observed in *C. elegans* embryos and even when the division directions were modified and the particular cell trajectories diverged from those seen in wildtype, the

overall packing stayed constant with the individual cells being switched within the diamond. Fickentscher and colleagues point out that "gross cellular arrangement is solely determined by mechanical constraints"[15].

More recently, in 2016, Fickentscher and colleagues[16] modified their simulation to include a volume-dependent division time inspired by the observed anti-correlation between division time and cell size in *C. elegans*. Along with a longer SPIM timelapse of the embryo, the augmented simulator was now able to match the early embryo cell trajectories up to the 24-cell stage (just before the onset of gastrulation). Fickentscher and colleagues tried two perturbations to their simulation to probe the embryo's resilience. First, all cells were forced to be symmetrical, but kept the division times that were predicted for their wildtype asymmetrical volume. The simulated embryo was found to always develop normally. Then, the cells were allowed to maintain the wildtype volume asymmetry, but the P1 derived cells were given the same timing volume-scaling rule as the other cells (instead of having a different empirically observed constant). Now, 10% of the simulations were observed to have an incorrect phenotype at the 24-cell stage. The cause was proposed to be a lack of time for cells to fully relax to wildtype positions before other cells divided again. The changed timings lessened the offset between the P1 and AB divisions which were required in wiltype development to give cells time to dynamically move to their expected next positions which introduced further positioning errors when the next division occurred.

Yamamoto and Kimura[72] adapted the model from Fickentscher *et al.* (2013) to

simulate the cellular packings that would occur if the aspect ratio of the eggshell were changed (Fig 1.4c). They sought to test if the diversity in cellular packings observed in the early embryos of different nematode species (and the robustness of the pattern within species) was caused by differences in the shape of the eggshells which varied in aspect ratio. Furthermore, Yamamoto and Kimura wished to simulate the effects of their experiments genetically modifying the aspect ratio of the eggshell of *C. elegans*. First, the same model with a repulsive-only force, total cell volume equal to the shell volume, and wildtype division rules was used and the shell aspect ratio was varied. The model was able to reproduce the observed packings at some aspect ratio, but did not match at high aspect ratios where the model would predict a linear arrangement when T-shaped arrangements were observed in experiments.

Based on observations of *C. elegans* embryos with removed shells, Yamamoto and Kimura changed the cell-cell interaction potential from repulsive-only to an adhesive potential leading the simulations to match the observed arrangements at various aspect ratios. The effect of changing division rules on the observed packings was also studied. Simulations were run with division rules other than the wildtype T-division rule that were displayed by *par2* and *par3* RNAi embryos and different simulated arrangement frequencies were observed that were qualitatively similar to those found in experiments.

At the other end of the simulation spectrum, the detailed equilibrium cell shape approach is exemplified by the work of Pierre *et al.*[45] where they sought to combine the surface energy minimizing package Surface Evolver[10] with a detailed microtubule-

length based model for division plane positioning augmented by extra terms to account for yolk gradients and polarity cues present in cells allowing for the iterated determination of cell positions, shapes and the positioning of daughters after division (Fig 1.4d). Using this framework, their simulations recapitulate the complex division patterns observed in diverse embryos from zebrafish to amphibians, sea urchins and ascidians in wildtype and under various experimental perturbations including deformation and centrifugation.

While the above works have strikingly shown the power of physical models to recapitulate early embryonic arrangements and division rules, there has not yet been a systematic study of how various physical parameters affect the cellular packings of soft adhesive spheres. Seeking to study these cellular packings, we have developed a computationally tractable, non-equilibrium Langevin simulation with a novel method of cell neighbor determination utilizing 3D Voronoi tessellation[52]. In the regimes of strong adhesion and strong confinement, distance-based metrics to determine neighbors are unreliable necessitating our approach.

1.5 Outline of dissertation

The focus of this dissertation is the use of a novel 3D Voronoi-augmented Langevin simulator to study the cell packings and cell arrangements that result from systematically varying the speed of divisions, division rules, the amount of external confinement by a shell, the strength of cell-cell and cell-shell adhesion and the aspect ratio of the confining shell.

1. In Chapter 2, I simulate the packings that result from changing the timing between divisions, the division rules (ordered and random) and the cell-cell adhesion strength in unconfined and confined settings. In the unconfined case, many packings besides the tetrahedron persist for very long times due to the embryo getting trapped in a floppy mode. By confining the cell cluster with a repulsive shell and studying the effects of decreasing the shell volume, I find there exists a shell volume where it is possible to override division rules and quickly relax cells to a specific arrangement. By varying the aspect ratio of the shell from a sphere to a long ellipsoid, one can robustly transition from a tetrahedral arrangement to a diamond and finally a line packing. Finally, by changing the shell from repulsive to sticky, new packings like the square are observed. Overall, confinement gives a robust and simple way to specify early embryo cell packings.

2. In Chapter 3, I focus on how division timing and division rules guide individual cells into proper arrangements within a well-defined cell packing. I restrict my attention to the early *C. elegans* embryo which takes on a diamond arrangement and has a specific arrangement of cells within that diamond, and study how robust the correct arrangement is to noise in the timing of divisions, in the angles of divisions, and to changes in the timing offset between when AB and P1 divide. The embryo turns out to be perfectly robust to moderate amounts of timing and angle noise and to have two separate types of error: arrangement errors resulting mainly from division angle noise and division sequence errors caused by timing noise. Shifts in the AB-P1

timing offset only cause non-lethal ABa-ABp rearrangements for moderate amounts of timing and angle noise. Finally, I systematically vary the division angles of AB and P1 and map out the final arrangements that each pair of angles leads to.

3. In Chapter 4, I synthesize the main conclusions of Chapters 2-3 and suggest future directions to extend the work described here.

Chapter 2

Blastomere packings under confinement

2.1 Introduction

During the initial stages of embryogenesis, when the number of cells (blastomeres) is very small, the spatial arrangement of blastomeres is essential for the proper development of the organism. This is particularly important in species, such as ascidians, nematodes, echinoderms and mammals, whose eggs are fully divided into blastomeres (cells) at the the initial stages upon fertilization, a process called holoblastic cleavage. In embryos of these species, the spatial arrangements of blastomeres upon successive cell divisions are critical because they define the neighbors of each cell and, consequently, the signals received by each blastomere [54], thereby controlling cell type specification. In nematodes (e.g., *C.*

elegans) it is well established that proper contact-mediated Notch-Delta signaling between blasotmeres [49], which depends on the proper blastomere arrangements and their neighbor relations, is critical for the survival of the embryo. While blastomere arrangements are stereotypical for a given species, they vary substantially across species [19]. This simultaneous intraspecies robustness and interspecies variation is apparent from the early blastomere arrangements (as early as the 4-cell stage) in nematodes [57, 21], echinoderms[19, 37], and even mammals[46, 18, 23] (Fig. 2.1A).

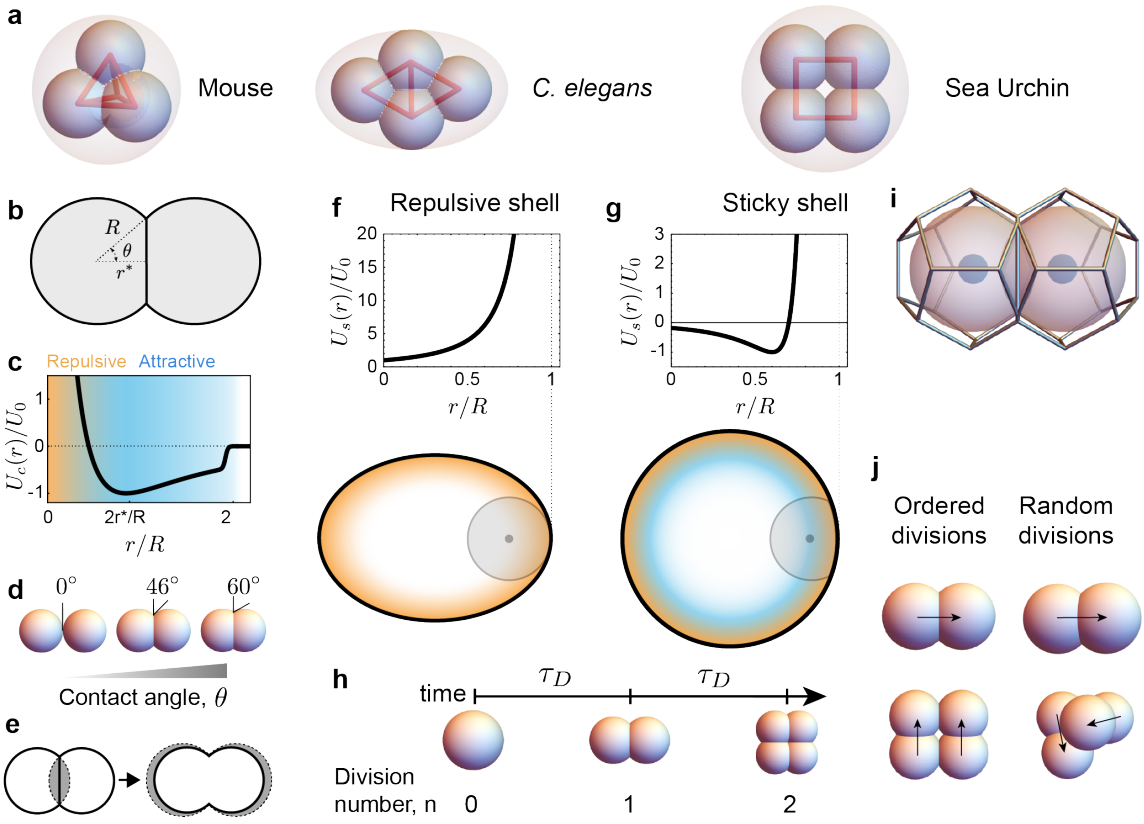

Figure 2.1: **Schematic diagrams of early embryo modeling** A: Illustrations of the most common 4-cell embryo arrangements in the mouse (a tetrahedron), *C. elegans* (a diamond) and the sea urchin (a square). Blue spheres represent blastomeres and the pink surrounding ellipsoid represents the confining envelope (vitelline envelope, hard chitinous egg shell, or hyaline layer) present for each embryo. B: Abstraction of cells to central points with contact size R,

equilibrium distance $2r^*$ and contact angle θ. C: Increasing the contact angle represents a relative increase of adhesion between cells. Here are shown contact angles of 0 degrees, 46 degrees and 60 degrees. D: The radial potential between two cells has a cutoff distance at $2R$, an attractive region from $2R$ to $2r^*$ and a repulsive region within a distance of $2r^*$. The minimum of the potential is normalized to -1. E: The overlapping region interpenetrating a neighboring cell is added back to each cell leading in an increased contact radius R'. F: A contour diagram of the repulsive potential used for the confining shell with orange values being greater than blue values. (Here the shell has an aspect ratio of 1.) The inset shows the radial one-dimensional form of this potential which diverges at the shell. G: A contour diagram of the attractive potential used for the confining shell with orange values being greater than blue values. (Here the shell has an aspect ratio of 1.) The inset shows the radial one-dimensional form of this potential which has a minimum at $L_b - r^*$ and that diverges at the shell boundary. H: An illustration of the time τ_D between cell divisions. (All cells divide at the same time in this model.) Total volume is conserved so each division decreases the cell radii proportionately. I: 3D Voronoi tessellation starting with dodecahedra that surround a sphere of size R_n are used in conjunction with distance to determine cell neighbors. J: Simulations following the ordered division rule divide from 1 to 2 cells in the x direction and then from 2 to 4 in the y direction. For the random division rule, each daughter cell divides in a random direction.

The spatial arrangement of blastomeres in early embryos, as well as their dynamics, are ultimately controlled by their physical interactions. Cell adhesion between blastomeres helps them stick together and the balance between cortical actomyosin activity and adhesion is thought to establish the contact surface between blastomeres or, alternatively, the contact angle between them. If these were the only factors determining the arrangement of blastomeres, then the problem would be equivalent to the packing problem of a cluster of particles [64, 26], which has been studied from both mathematical [60, 2, 31, 43, 25] and physics perspectives[38, 26, 36]. In this case, the expected cellular packing configuration (spatial blastomere arrangement) at the 4-cell stage would be a tetrahedron. While this is indeed the observed packing configuration at the 4-cell stage in mammals, the 4-cell stage packings in nematodes, ascidians, echinoderms, etc., are not tetrahedral [19]. Since the tetrahedral packing corresponds to the lowest energy

state (equilibrium configuration) in particle packings, the observation of 4-cell stage packings that strongly differ from the tetrahedral arrangement indicates that either there are additional forces (beyond cell-cell interactions) affecting the blastomere equilibrium configuration, that the observed packings are metastable states with long relaxation times or that the blastomere packings are actively maintained in non-equilibrium configurations.

Beyond the direct physical interactions between blastomeres, recent experiments in *C. elegans* embryos have shown that physical confinement by the eggshell affects blastomere arrangements [72], and several other works have highlighted the important role of division rules (i.e., the rules that define the orientation of the blastomere division planes) in blastomere arrangements [45]. The existence of cell divisions with controlled spatial orientations could maintain the system out-of-equilibrium and potentially control blastomere packings.

Previous theoretical works simulating blastomere packings have either used particle based models or surface energy minimization in conjunction with a shape dependent model of division plane positioning. In Fickentscher et al. (2013)[15] and Fickentscher et al. (2016)[16], early blastomere dynamics in *C. elegans* were modeled using repulsive soft spheres confined by an ellipsoidal shell. Blastomere trajectories between divisions were found to match those observed by single plane illumination microscopy (SPIM) in real C. elegans embryos up to the 12-cell stage and 24-cell stage when using volume-dependent division timing and longer imaging. Yamamoto and Kimura[72] adapted the Fickentscher et al. (2013) model to study the diverse 4-cell arrangements found between

different species of nematodes and to model their experiments changing the aspect ratio of *C. elegans* eggshells. They included differential adhesion between blastomeres and varied the aspect ratio of the repulsive eggshell finding that the dominant blastomere arrangement at the 4 cell stage varied depending on the aspect ratio and division rules. However, all these particle based models mainly studied embryos where the volume of all blastomeres was equal to the egg shell volume.

Here we sought to systematically study how the physical confinement of the early embryo, the existence of division rules and the change in adhesion strength between blastomeres control the cellular packings (blastomere arrangements) of 4-cell stage holoblastic embryos. We focus on the 4-cell stage because the observed variability across species is large, while being a tractable problem from a combinatorial (computational) perspective. By simulating the dynamics of the cells in 3D, and using Voronoi tessellation to determine the neighbor relations between blastomeres (topology of cell contacts), we find that in the absence of embryo confinement the division rules and the timing between division play an important role in the packing configurations. However, in embryos for which the confinement is non-negligible (as in most cases of holoblastic cleavage), the geometry of the confining shell is the main factor in the determination of the cellular packings, overriding division rules.

2.2 Methods

Numerical Simulation

The 3D Langevin equations (Eq. 2.8) governing the motion of cells were solved via the Euler-Maruyama method [28]. Simulations were run using a timestep $\Delta t \equiv 10^{-3}\tau_R$, much smaller than all relevant timescales in the system, namely τ_R and τ_D. The discretized version of Eq. 2.8 integrated numerically reads

$$\vec{r}_i(t+\Delta t) = \vec{r}_i(t) - \sum_{j\in\Omega_i^t} \partial_{r_{ij}} \tilde{U}(r_{ij};\,\theta)\,\Delta t + \sqrt{2\sigma\Delta t}\,\vec{\eta}\,, \tag{2.1}$$

where θ are the cell-cell potential parameters (Methods), σ is the random noise scale (set to 5×10^{-5}), $\vec{\eta}$ is a standard normal random vector with each component drawn from $\mathcal{N}(0,1)$ and Ω_i^t is the set of cells in direct contact with cell i at time t. The elements of the set Ω_i^t are obtained from the Voronoi tessellation of the system at time t (Methods).

Simulations were initialized with the undivided egg (first cell) at the origin for unconfined simulations or to have Gaussian distributed initial positions with variance $b/10$ around the origin for confined simulations. Simulations either ended at the timestep before cells at the 4-cell stage would divide again for non-equilibrium simulations, when 4 cells reached a tetrahedron in simulations searching for the equilibrium relaxation time, or after $8000\,\tau$ to determine equilibrium configurations in embryos with confining shells.

Cell-cell interaction potential

The cell-cell interaction potential has a Lennard-Jones like form, but is multiplied by a support function that cuts it off at a given distance while keeping it continuous and differentiable (Fig 2.1d). The cutoff distance for a given cell pair i and j is set to $R_i + R_j \equiv R_{ij}$, with R_i and R_j being the radii of cells i and j, respectively. The size of each cell (or the radius equivalently) can be different because of the volume conservation correction and because of cell divisions (see Methods below). The potential has an equilibrium distance $r_i^* + r_j^* \equiv r_{ij}^*$ (Fig 2.1b) which is the equilibrium distance between two cells combining the equilibrium radii of each cell. The form of the cell-cell potential is

$$U(r_{ij}; r_{ij}^*, R_{ij}) = \frac{U_0}{(\alpha - \beta)} \left[\frac{1}{1 + f(r_{ij})} \right] \times \left[\frac{(r_{ij}^*)^\alpha (\beta + f(r_{ij}^*) \left[\beta + \frac{r_{ij}^*}{\tilde{a}} \right])}{r_{ij}^\alpha} - \frac{(r_{ij}^*)^\beta (\alpha + f(r_{ij}^*) \left[\alpha + \frac{r_{ij}^*}{\tilde{a}} \right])}{r_{ij}^\beta} \right], \quad (2.2)$$

where the α, β, and a are parameters characterizing the shape of the potential and the cutoff support function, U_0 is the energy scale of the potential (the potential equals -U_0 at its minimum) and $f(r_{ij}) \equiv e^{\frac{(r_{ij} - R_{ij})}{a}}$. We set $\alpha = 4$, $\beta = 3$, and $\tilde{a} = 0.01$.

Confining Shell

The shape of an axisymmetric ellipsoidal shell, and the associated ellipsoidal level set, are given implicitly by

$$\frac{x^2}{a^2} + \frac{y^2}{b^2} + \frac{z^2}{b^2} = c\,, \tag{2.3}$$

where a is the length of the ellipsoid's major axis, b is the length of its minor axis and$c$ is a positive constant that defines the ellipsoidal level set where $c = 1$ defines the shell itself.

Since cells cannot penetrate the shell, the confining potential must diverge at the positions where the shell is located ($c = 1$). Moreover, the potential must vanish when the cell can no longer be in contact with the shell, which occurs when a cell is located at a distance larger than R from the shell. With this in mind, we define the confining potential of a repulsive shell U_{rs} (Fig 2.1f) as

$$U_{rs}(x, y, z; R, k_{shell}) = \frac{k_{shell}}{1 - \sqrt{\frac{x^2}{a^2} + \frac{y^2}{b^2} + \frac{z^2}{b^2}}}\,\Theta\left(\sqrt{\frac{x^2}{a^2} + \frac{y^2}{b^2} + \frac{z^2}{b^2}} - (1 - \frac{R}{b})\right) \tag{2.4}$$

where k_{shell} is the energy scale of the shell potential and $\Theta()$ is the Heaviside step function that sets the function to zero when a cell is too far from the shell to be in contact. We used a Heaviside step function instead of using a support function to cut off the potential above cell size for mathematical convenience. We set $k_{shell} = 10$ to balance the repulsion forces between two cells and between cells and the shell when in steady state confinement.

The force acting on cell i arising from contact with the shell is given by

$$\vec{F}_i^s = -\nabla U_{rs}(\vec{r}_i)\,, \tag{2.5}$$

where $\vec{r}_i$ is the position of cell i.

In the case of a sticky shell (Fig 2.1g), we use the same shell-cell interaction potential as the interaction potential between 2 cells, albeit with different adhesion strength. In this case, the equilibrium distance is changed to r_i^* instead of $r_i^* + r_j^*$ since there is only one cell interacting with the shell. In these conditions, the interaction potential for a sticky shell reads

$$U_{ss}(x,y,z;r_i^*) = \frac{U_s}{(\alpha-\beta)}\left[\frac{\beta(r_i^*)^\alpha}{(1-\sqrt{\frac{x^2}{a^2}+\frac{y^2}{b^2}+\frac{z^2}{b^2}})^\alpha} - \frac{\alpha(r_i^*)^\beta}{(1-\sqrt{\frac{x^2}{a^2}+\frac{y^2}{b^2}+\frac{z^2}{b^2}})^\beta}\right] \Theta\left(\sqrt{\frac{x^2}{a^2}+\frac{y^2}{b^2}+\frac{z^2}{b^2}} - (1-\frac{R}{b})\right) \tag{2.6}$$

where U_s is the adhesion energy scale. The effect of the potential was examined at adhesion energy values U_s of 0.2, 0.4, 0.6, 0.8, 1, 2, 4, 6, 8, 10, 15, and 20.

Topology Inference

Because we simulated particles in a confined volume, it was necessary to move beyond a simple distance metric to determine if two cells were neighbors. We use a 3D Voronoi partitioning as an extra constraint in addition to distances. The package we used,

Voro++[52], determines the 3D Voronoi polytope around each cell by starting with a large 3D volume and then cutting it using the midplanes from the current cell to each of its neighbors. In this work, each cell starts with a dodecahedral volume that surrounds an inscribed sphere with the cell radius R. When a pair of cells are close enough, their dodecahedral volumes are cut by the weighted midplane between them (adjusted from the midpoint by their respective radii) (Fig. 2.1j). Each new cut face of the Voronoi polytope is identified with a neighboring cell allowing all neighbors to be identified. Using a 3D Voronoi partition is critical to properly detect when cells are not in contact even when they are within the contact distance due to blocking by neighboring cells. It was also necessary to have the square arrangement of cells be distinguishable from the tetrahedron since with soft spheres, both cases have all cells within the contact distances of all others. Finally, using the 3D Voronoi to determine neighbors is critical to avoid soft spheres unphysically always forming a tetrahedron when strongly confined.

Two cells are defined to be in contact when they are within R_{ij} of each other and their Voronoi polytopes share a face. An adjacency graph is created by defining each cell as a node and adding edges between each pair of cells found to be in contact. Since we are only interested in the overall topology of the cell arrangement and not the precise position of each cell in the arrangement, we determine the topology of each arrangement by checking if the adjacency graph is isomorphic to a reference adjacency graph for each type of topology (square, diamond, tetrahedron, T-shape, line)[2, 69].

Cell Divisions

Cell divisions occur at well defined intervals of time τ_D (Fig. 2.1h), with all cells dividing simultaneously. The new daughter cells were placed a radius away from the mother cell in a single timestep (Fig. 2.1i). In the case of random divisions, the daughter cell divides in a random direction from the mother cell (with a check to ensure that the daughter is not placed within a distance that would cause it to substantially overlap with an already existing cell ($< R_n$) for an nth division daughter). For the case of ordered divisions, the egg first divides in the x direction, then both daughter cells divide in the y direction.

The total cell volume is conserved so the two daughter cells each have half the volume of the mother cell, as described in the main text.

Volume Adjustment

The overlap between blastomeres was determined by defining a sphere with radius R_i around each cell i and then calculating its overlap volume V_o with neighboring spheres. This overlapping volume is added to cell i, making its size larger. In particular, the radius of cell i is modified from R_i before the correction to R_i' after it, with $4\pi(R_i')^3/3 = 4\pi(R_i)^3/3 + V_o$ (Fig 2.1e). This adjustment is performed once per timestep. The Voronoi dodecahedron is also scaled to surround a sphere of radius R_i' after volume correction.

Angular Mean Squared Displacement

The angular mean squared displacement is defined as

$$MSD(t) = \langle (\theta(t) - \theta(0))^2 \rangle \,, \tag{2.7}$$

where $\theta(t)$ is the angle of a blastomere relative to three cells forming a triangle in the x-y plane.

2.3 Results

Theoretical Description

In order to simulate the 3D dynamics of blastomeres, accounting for the interactions between them, their divisions as well as embryo confinement, we use a minimal representation and describe each blastomere (cell) as a particle. Particle-based descriptions have previously been used to describe blastomere motion in early *C. elegans* embryos and shown to properly describe cellular movements [15, 16, 72]. In this particle-based representation, cells interact with each other through an interaction potential $U(r_{ij})$ that effectively accounts for the mechanical interactions between cells (adhesion, etc. [44]), with $r_{ij} = |\vec{r}_i - \vec{r}_j|$ being the distance between two given cells located at positions $\vec{r}_i$ and $\vec{r}_j$. Cell-cell adhesion is represented by an attractive range in the potential, whereas a repulsive region ensures that cells do not interpenetrate when they become too close to

each other (Fig. 2.1b). To account for cell size in this particle description, we include a sharp cut-off of the potential at a distance R, which corresponds to the radius of an isolated blastomere. The balance of attractive and repulsive forces between two blastomeres occurs when they are separated by a distance $2r^*$. The ratio between this equilibrium distance between blastomeres and the blastomere size $2R$ corresponds to $r^*/R = \cos\theta$, with θ being the contact angle between cells (Fig. 2.1c,d). Since the contact angle is an easily measurable quantity that informs about the relative strength of adhesion and cortical tension [35, 72], we use θ as control parameter instead of r^*. Moreover, although it is not possible to enforce exact volume conservation in a particle-based description, we perform leading order corrections upon cell contact (Fig. 2.1e; Methods); we have checked that the volume corrections are small and we have tested that our results do not qualitatively depend on them.

At the spatial and temporal scales of embryo development, the system is overdamped and inertia can be safely neglected [50]. In this case, force balance (momentum conservation) for a given blastomere reads

$$\mu \frac{d\vec{r}_i}{dt} = \sum_{j \neq i} \vec{F}^c_{ij} + \vec{F}^s_i + \vec{\eta}_i \,, \tag{2.8}$$

where $\vec{r}_i$ is the position of cell i in 3D, $\vec{F}^c_{ij} = -\nabla U(r_{ij})$ are the forces that cells in contact apply on each other, $\vec{F}^s_i$ represents the force of a confining shell on cell i (whenever a confining shell is present), and $\vec{\eta}_i$ is a small fluctuating force (Gaussian white noise) that is meant to represent the force fluctuations acting on cells. Finally, the parameter μ

corresponds to a friction coefficient that resists cell movement in an overdamped environment and it is here assumed constant and the same for all blastomeres. To obtain the force $\vec{F}_i^s$ from the confining shell on cell i, we define the geometry of the confining shell and set the interaction potential $U_{\text{shell}}(x, y, z)$ that a cell would perceive inside the shell (Fig. 2.1f,g; Methods). The confinement force perceived by cell i is then given by $\vec{F}_i^s = -\nabla U_{\text{shell}}(x, y, z)$ (Methods).

In order to properly determine what cells are in contact and can therefore apply forces on each other, we use Voronoi tessellation (Methods; Fig. 2.1j). Previous particle-based simulations have use distance-based metrics to determine the neighbors of each cell. However, distance-based metrics give erroneous results for both cell-cell contacts and dynamics in the presence of confining shells. This is because when cells are highly confined, the distance between next-nearest neighbors can be smaller than the interaction potential range, thereby erroneously considering the forces of cells that are not in direct contact. Voronoi tessellation overcomes this problem and enables proper determination of cell-cell contact topology at each timestep of the simulation (Methods).

Since shells of many species have spherical or ellipsoidal shapes, we consider only these cases in what follows. We approximate the shell surrounding the embryo by an axisymmetric ellipsoid with major and minor axes a and b, respectively, with volume $V_s = \frac{4\pi}{3}ab^2$ and aspect ratio a/b. Since blastomeres cannot penetrate the shell, we used confining potential forms that diverge at the shell boundary (Methods; Fig. 2.1f,g). Moreover, the confining potential vanishes for distances larger than R from the shell, as

these are not within the reach of cells.

Beyond physical interactions among cells and with the confining shell, blastomeres in early embryos divide at regular intervals, with a time τ_D between division events (Fig. 2.1h). We simulate division events (Methods) accounting for the change in volume of the cells upon division. Since the volume of the daughter cells is half of cell volume before division, the cell radius R changes after each division cycle to $R_n = R_0/2^{n/3}$, where R_0 is the radius of the initial egg (and $V_c = 4\pi {R_0}^3/3$ is the initial egg volume) and n is the number of divisions that have occurred (Fig. 2.1h). Finally, in order to study the role of division rules, we control the spatial direction along which the division occurs (perpendicular to the mitotic plane [41, 20]). While division rules are known to exist, the specific rules and the parameters that control them are still under debate, especially for different species [22]. As a consequence, to study the role of division rules, we consider two limiting cases: (1) *Ordered divisions*, in which we impose representative division rules at early developmental stages (division axis is perpendicular to the division axis in the two previous divisions; for first division, only perpendicular to previous division), and (2) *Random divisions*, in which there are no division rules and we randomize the direction of cell divisions for each cell and division cycle(Fig. 2.1i).

Normalizing all lengths by the initial egg radius R_0, all forces with U_0/R_0 and time with the mechanical relaxation time τ_M, which is given by $\tau_M \equiv \mu R_0^2/U_0$ and represents the characteristic timescale over which mechanical disturbances typically relax to equilibrium, the relevant dimensionless parameters in the problem are θ, τ_D/τ_M, V_s/V_c,

U_s/U_0, and γ where $\theta = \cos^{-1}(r_i^*/R_i)$ is the contact angle, τ_D/τ_R is the ratio of the time between divisions to the mechanical relaxation timescale, $V_s/V_c = \gamma(L_b/R_0)^3$ is the ratio of the shell volume V_s to the total cell volume V_c, U_s/U_0 is the ratio of the energy scale of the minimum of the attractive cell-shell potential and the cell-cell potential, and $\gamma = L_a/L_b$ is the aspect ratio of the shell.

Dimensionless Parameters	
Parameter	Description
θ	*Contact angle*: Specifies the relative strength of adhesion between cells to the cortical tension of each cell
τ_D/τ_M	*Division time ratio*: Duration of the time between divisions relative to the mechanical relaxation time
V_s/V_c	*Volume ratio*: Ratio of confining shell volume and the total volume of cells
U_s/U_0	*Adhesion strength ratio*: Ratio of the adhesion potential scale between a cell and the confining shell compared to the adhesion strength between cells
a/b	*Shell aspect ratio*: Ratio of ellipsoid major axis length a to minor axis length b

Table 2.1: Definition of the relevant dimensionless parameters in the problem.

In what follows, we simulate the stochastic movements of the multiple interacting blastomeres using Langevin dynamics (Eq. 2.8; Methods) in different conditions .

Unconfined Cellular Packings

To understand the packing configurations at the 4-cell stage that arise from the non-equilibrium dynamics, we first simulate the cellular dynamics upon divisions in the ab-

sence of embryo confinement (Fig. 2.2a,c). We define the 4-cell stage packing configuration as the cellular arrangement just before cells at the 4-cell stage undergo the next division(Fig. 2.2b). At equilibrium, the minimal energy configuration of 4 blastomeres in contact with each other is a tetrahedron, as already established both theoretically and experimentally for clusters of four particles with attractive interactions [60, 2, 31, 38]. However, if blastomeres divide much faster than the time required for cells to undergo mechanical relaxation ($\tau_D \ll \tau_R$), cells do not have time to reach mechanical equilibrium in between divisions and the cellular packings do not coincide with the equilibrium packing, as expected. When divisions are fast compared to mechanical relaxation ($\tau_D/\tau_R = 0.1$; Fig. 2.2c) and cells divide according to ordered division, either squared or diamond configurations are observed, with diamond configurations being more prevalent as the cell contact angle increases. If cells divide in random directions, other packing configurations appear and depend on the contact angle, but both squared and tetrahedral packings are missing. In contrast to the case where division occur fast compared to mechanical relaxation, if blastomeres take mach longer to divide than the mechanical relaxation time, equilibrium packings are expected because cells should have enough time to reach mechanical equilibrium in between divisions. However, our simulations show that for $\tau_D \gg \tau_R$ (specifically, $\tau_D/\tau_R = 10$), the expected tetrahedral configurations are not observed for ordered divisions (only diamond configurations are observed) and barely observed for random divisions.

To understand why the expected tetrahedral configurations are not observed, we char-

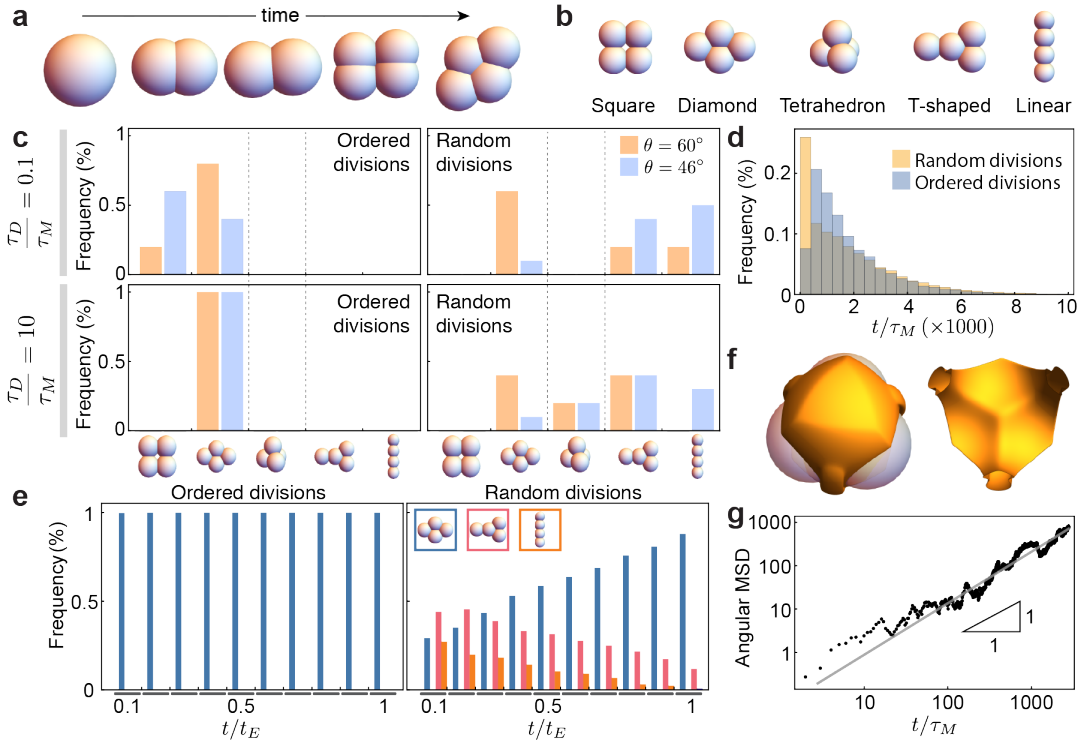

Figure 2.2: **Unconfined Cellular Packings.** A: Snapshots of a simulation following ordered division rules and with slow divisions ($\tau_D/\tau_M = 10$) showing the egg, two cells right after division and after reaching equilibrium and four cells right after division and right before the next division. B: Arrangement topologies for four cells were categorized as square, diamond, tetrahedron, T-shaped or linear. C: comparison of the frequency of cell arrangements for slow and fast divisions ($\tau_D/\tau_M = 0.1, 10$) and divisions using ordered or random division rules. Red lines indicate the minimal energy tetrahedral arrangement. Orange bars indicate a contact angle of 60 degrees and blue of 45 degrees. D: A histogram of the time to reach equilibrium for 100,000 simulations. Times are scaled by $1000\tau_M$. E: Two figures showing how long embryos remain in different arrangements before they reach the tetrahedral arrangement for ordered and random division rules.. Histograms show the frequency of different arrangements at various relative times normalized by the final time needed to reach equilibrium. F: A top view (with cells) and cross section (without cells) showing the three dimensional potential caused by three cells on a fourth cell (with potential value near -2) indicating the directions that the fourth cell can move with no net force. G: A log-log plot of the angular mean squared displacement of a fourth cell interacting with three held fixed in a triangle. The black line indicates a slope 1 that represents diffusion. The red line indicates a non-linear fit of the simulated angular MSD with a slope of 1.19.

acterized the time necessary to reach the tetrahedral equilibrium configurations at the 4-cell stage (by preventing the next division round). Both for ordered and random divi-

sions, we find that cells require times three orders of magnitude longer than τ_R to reach equilibrium (Fig. 2.2d). By monitoring the time evolution of packing configurations at the 4-cell stage as the system relaxes to equilibrium, we found that for ordered divisions cells are always in a diamond configuration before reaching the tetrahedral configuration, whereas for random divisions cells evolve towards the diamond configuration and stay in that configuration until reaching the equilibrium packing (with a few clusters transiting directly from a T-like configuration to the tetrahedral state) (Fig. 2.2e). This results indicate that it takes a long time for the cluster to leave the diamond configuration, suggesting that the transition between diamond and tetrahedral configurations may involve the rotational diffusion of a blastomere. Indeed, the equipotential surface that a blastomere perceives when the three other form a triangle indicates that to transit from diamond to tetrahedral configurations, one blastomere needs to traverse a flat region of the potential (Fig. 2.2f). The angular mean squared displacement of the movements of such blastomere scales linearly with time (Fig. 2.2g), showing that the transition between diamond and tetrahedral configurations occurs via rotational diffusion and explaining the long times necessary to reach the tetrahedral state. The consequence of this floppy mode in the dynamics of the blastomeres is that it imposes an extraordinarily long time for the system to reach mechanical equilibrium, effectively leading to a degeneracy the the packing configurations at the 4-cell stage for normal division times, with degenerate packings being strongly dependent of division rules and adhesion strength between blastomeres. Such large degeneracy in the packing configurations and their strong dependency of mul-

tiple parameters does not appear to be an adequate strategy to robustly specify cellular packings.

Since tetrahedral packings at the 4-cell stage are observed in embryos of several species, our results suggest that another mechanism must contribute to establishing the observed tetrahedral packings, as otherwise cell divisions would need to be extraordinarily slow ($\tau_D \sim 24$h) to allow blastomeres to reach equilibrium between divisions.

Cellular Packings under Spherical Confinement

Many embryos displaying tetrahedral packings at the 4-cell stage seem to have a spherical confining shell [57, 72]. To understand the potential role of embryo confinement on cellular packings at the 4-cell stage, we simulate the dynamics of blastomeres in the presence of spherical confinement. We focus on long division times ($\tau_D/\tau_R = 10$) as this was the limit in which tetrahedral packings were expected, but shown above to be missing due to the long times associated with rotational diffusion of the blastomeres. If the confining shell has a very large volume compared to the total volume of the cells ($V_s \gg V_c$; Fig. 2.3a), the situation is similar to the unconstrained embryo (although the linear arrangement is suppressed). As the volume of the confining shell is decreased, the 4-cell stage packings start to change because cells start interacting with the shell. Finally, when the volume of the confining shell is comparable to the volume occupied by the cells (but larger; $V_s \simeq 2V_c$), only tetrahedral configurations are observed (Fig. 2.3c). In this case, we find that the blastomeres robustly reach the tetrahedral packing at the

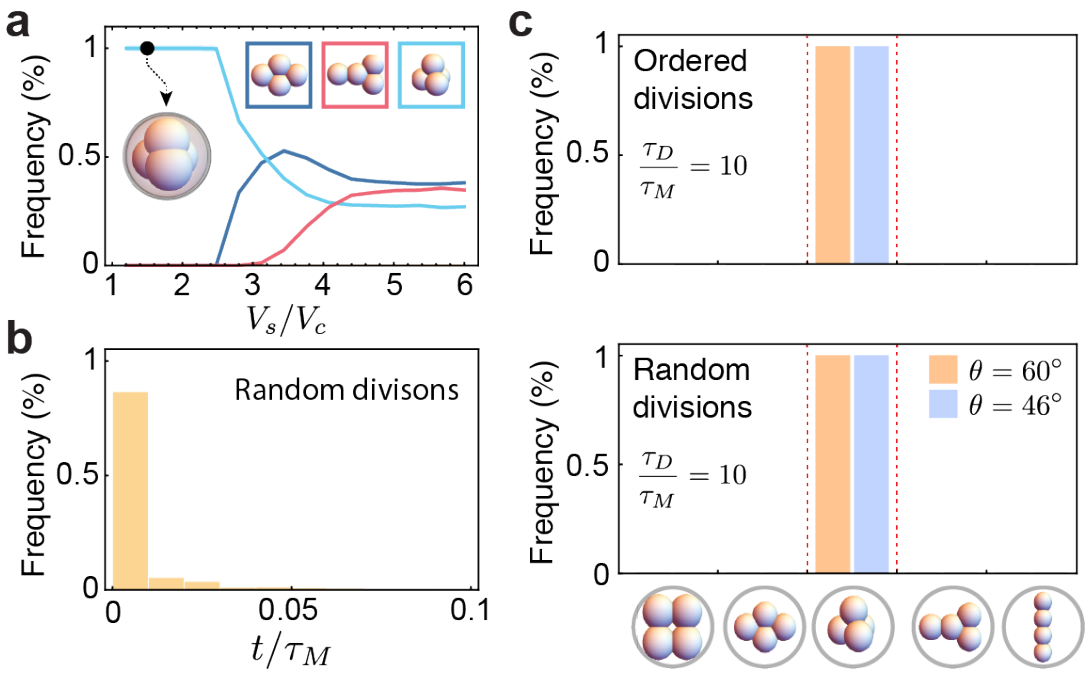

Figure 2.3: **Spherically Confined Packings.** A: Frequency of arrangements for random division rule, slow division simulations as volume ratio is decreased for embryos with spherical repulsive confinement. The gray bar at a volume ratio of 1.52 indicates the regime where the previous simulations were run. The colored lines include an error envelope that corresponds to $\pm$ one standard deviation assuming each datapoint came from a Poisson process (i.e. $\sqrt{N}$). B: Histogram of times to reach the tetrahedron for a spherically confined simulation with volume ratio of 1.52. Unlike with the unconfined case, now all 1000 simulations reach the tetrahedral arrangement within $0.1\tau_M$.
C: Frequency of arrangements for spherically confined simulations with slow divisions ($\tau_D/\tau_M = 10$), a repulsive confining shell with an aspect ratio of 1 and a volume ratio of 1.52. Now, 100% of the arrangements reach the tetrahedron by the end of the simulation for both contact angles (Orange bars indicate a contact angle of 60 degrees and blue of 45 degrees).

4-cell stage regardless of their contact angle or division rules. Moreover, they reach the tetrahedral packings within timescales smaller than τ_R and five orders of magnitude faster than in the absence of confinement (Fig. 2.3b). These results indicate that the presence of spherical confinement removes the degeneracy of cellular packings and imposes a tetrahedral blastomere configuration at the 4-cell stage, overriding division rules.

Cellular Packings under Ellipsoidal Confinement

While embryos of several species have spherical confining shells, other shell geometries are observed across species. Different nematode species display elongated axisymmetric shells of varying aspect ratios [57, 21] that can be approximated by an axisymmetric ellipsoidal geometry. Previous works have shown that the shape of the confining shell is important for cellular arrangements in nematodes [72]. In nematode species, the 4-cell stage packing arrangements are critical for the survival of the embryo, as improper cell contacts lead to fatal developmental defects [48]. To understand the role of varying ellipsoidal shell geometries on the cellular packings across nematode species, we systematically studied the effect of confining shell volume and aspect ratio on the blastomere packing configurations at the 4-cell stage.

For spherical shell geometries, we found that even when the time between divisions τ_D was considerably larger than the mechanical relaxation time τ_R, the resulting 4-cell stage packing ($\tau_D/\tau_R = 10$; Fig. 2.3a) was not the expected equilibrium packing if the volume of the shell was much larger than the total volume of the blastomeres (essentially, in the limit of negligible confinement), both for ordered and random divisions. Similarly, we find that for all simulated aspect ratios of ellipsoidal shells ($a/b = 1, ..., 3$; $\tau_D/\tau_R = 10$), when the confinement is negligible ($V_s/V_c \gg 1$), a strong degeneracy in packing configurations is observed in the case of random divisions, with similar relative frequencies for the different packing configurations, albeit with the diamond configuration always being predominant. Essentially, if the volume of the shell is sufficiently large compared to the total volume

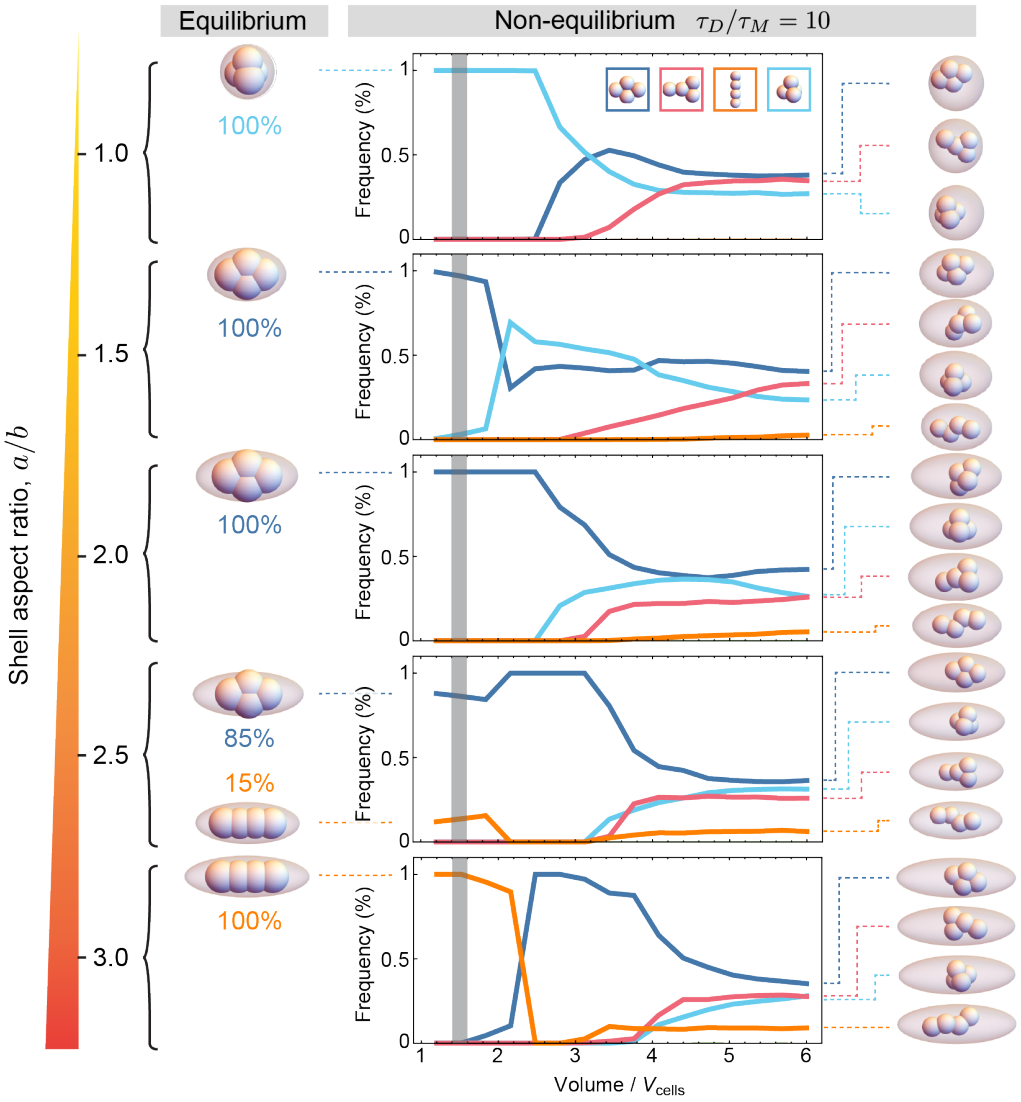

Figure 2.4: **Arrangements for Repulsive Confinement with Increasing Aspect Ratio.** (From right to left) Renderings on far right show respective arrangements present with a volume ratio of 6 for simulations with random division rules and slow divisions ($\tau_D/\tau_M = 10$) for all five aspect ratios from an aspect ratio of 1 at the top to an aspect ratio of 3 at the bottom. Colored lines indicate the frequencies of arrangements for decreasing shell volume ratios. The colored lines include an error envelope that corresponds to +/- one standard deviation assuming each datapoint came from a Poisson process (i.e. $\sqrt{N}$). (Far left) Renderings show the arrangements that persist at a volume ratio of 1.52 (indicated by the gray bar) after waiting $8000\tau_M$. The relative frequency observed at the end of 200 simulations. These long-lived configurations change with increasing aspect ratio as shown with only an aspect ratio of 2.5 having two metastable states.

of the blastomeres ($V_s/V_c \gg 1$), the observed packings at the 4-cell stage are similar to unconfined embryos (Figs. 2.2a and 2.4), as should be expected. As the volume of the shell is decreased and the blastomeres start to feel the physical confinement, the relative frequencies of 4-cell stage packings start to change, removing some degeneracy in packing configurations, in a manner that depends on the shell aspect ratio. Similarly to the spherical confinement case described above, when the volume of the confining shell is comparable to the volume occupied by the cells (but larger; $V_s \simeq 2V_c$), the degeneracy in 4-cell stage packings largely disappears and different, but unique, packings exist for different aspect ratios.

For some shell geometries (aspect ratios) we observe that even under confinement, two different packing geometries are possible, albeit with different relative frequencies. For aspect ratio of 1 (spherical limit), only tetrahedral packings are obtained, as described above and observed for nematode species with spherical shells [57, 72]. As the aspect ratio increases the relative frequency of the tetrahedral packing diminishes and the frequency of diamond packings increases. At aspect ratios $a/b \sim 1.5$, tetrahedral configurations are nearly fully suppressed and only diamond configurations are observed. Diamond packings are the only observed configuration up to aspect ratios of about $a/b \sim 2.4$. Increasing the aspect ratio above this value, leads to the coexistence of diamond and linear configurations. For aspect ratios of $a/b \sim 3$ and above, the only observed configuration is linear.

To check if the packing configurations obtained in confined embryos ($V_s/V_c = 1.52$;

$\tau_D/\tau_R = 10$) correspond to the actual equilibrium packings for each specific shell geometry, as was the case for the spherical shell, we simulate the dynamics of blastomeres, preventing further cells divisions at the 4-cell stage and letting the system reach equilibrium. We find that for each value of the aspect ratio, the packing configurations observed for $\tau_D/\tau_R = 10$ (with random divisions) were the actual equilibrium configurations of the blastomeres at the same confining volume ($V_s/V_c = 1.52$) and aspect ratio. This indicates that the confining shell eliminates the degeneracy in packings and selects the equilibrium packing configurations for a given shell geometry. These results indicate that the geometry of the confining shell alone can determine the 4-cell stage blastomere arrangements regardless of the specific division rules, providing a robust mechanism to remove packing degeneracy and select the proper cellular packing.

Cellular packings in sticky shells

So far, we have only considered shells that confined the blastomeres by generating a repulsion force upon contact. However, in some species, the blastomeres can adhere to the confining shell, likely affecting blastomere packing configurations. In the case of sea urchin embryos (echinoderms), there is evidence of strong adhesion to the hyaline layer surrounding the blastomeres [37, 1, 66] and the 4-cell stage blastomere packing configurations is a square [19], a configuration never observed in the cases described above. In the case of sea urchins, the geometry of the hyaline layer (confining shell) that surrounds the blastomeres is not exactly spherical and changes slightly over time. However, for the

sake of simplicity, here we consider an spherical sticky confining shell. Since echinoderms have stereotypical division rules (dividing perpendicular to the two previous divisions at early stages) we study the effect of shell-blastomere adhesion strength and confining volume on the 4-cell stage packing configurations for ordered divisions (Fig. 2.1i).

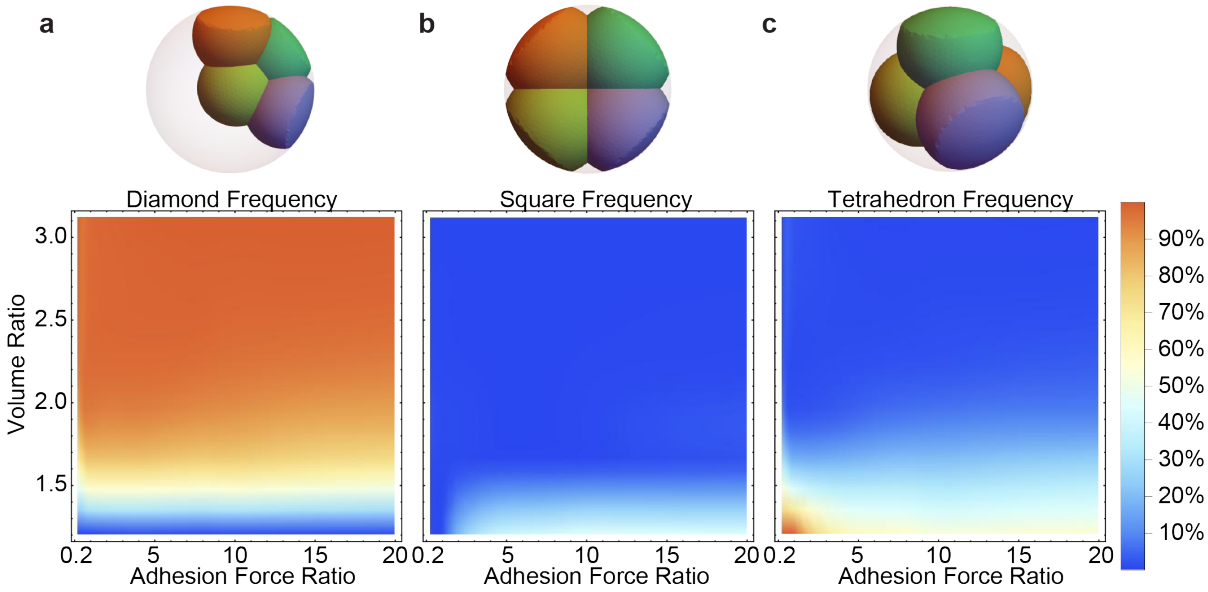

Figure 2.5: **Arrangements for Spherical Adhesive Confinement** A: (top) Rendering of the positions of 4 cells in the diamond arrangement within an adhesive spherical shell with a volume ratio of 3.12 and an adhesion force ratio of 20. (bottom) Density plot of the frequency of the diamond arrangement for various volume ratios from 1.2 to 3.12 and adhesion force ratios from 0.2 to 20 with 5000 simulations for each parameter. B: (top) Rendering of the positions of 4 cells in the square arrangement within an adhesive spherical shell with a volume ratio of 1.2 and an adhesion force ratio of 20. (bottom) Density plot of the frequency of the square arrangement for various volume ratios from 1.2 to 3.12 and adhesion force ratios from 0.2 to 20 with 5000 simulations for each parameter. C: (top) Rendering of the positions of 4 cells in the tetrahedral arrangement within an adhesive spherical shell with a volume ratio of 1.2 and an adhesion force ratio of 0.2. (bottom) Density plot of the frequency of the tetrahedral arrangement for various volume ratios from 1.2 to 3.12 and adhesion force ratios from 0.2 to 20 with 5000 simulations for each parameter.

For large shell volume compare to the total blastomere volume ($V_s/V_c \gg 1$), the

only observed configuration with finite blastomere-shell adhesion is the diamond configuration, with the blastomeres adhered to the shell (Fig. 2.5a-c). When the confining volume becomes comparable to the blastomeres volume ($V_s/V_c \simeq 1 - 1.5$), the diamond configuration is suppressed and the tetrahedral and square packing configurations coexist at different frequencies depending on the relative strength of cell-cell adhesion and cell-shell adhesion. When adhesion to the shell is very low, only tetrahedral configurations are observed, as expected in the limit of negligible shell adhesion (repulsive shell). When the adhesion to the shell dominates over cell-cell adhesion, we find that square and tetrahedral packing configurations are observed approximately 40% and 60% of the time, respectively.

Therefore, the existence of strong adhesion to the confining shell introduces square packing configurations that were not observed in purely repulsive confining shells. However, the blastomere adhesion to the shell cannot be the only reason why 4-cell stage embryos of echinoderm species are square, since there is a strong probability of tetrahedral packings even in the presence of adhesion.

2.4 Discussion

Proper blastomere arrangements in early embryogenesis, and in particular their topology of cell-cell contacts, are critical to ensure proper development. Here we presented a systematic study of the possible (non-equilibrium and equilibrium) packing configurations (cell arrangements) both in the absence and presence of a confining shell that physi-

cally restricts the movements of blastomeres. We find that the shape of the confining shell determines the blastomere packing configurations of 4-cell stage embryos, regardless of division rules, removing blastomere packing degeneracies that could lead to fatal developmental defects.

In the absence of a confining shell, we find that the relaxation time to reach the equilibrium configuration is extraordinarily long due to rotational diffusion of blastomeres. Blastomere divisions occurring before relaxation generate a considerable degeneracy of 4-cell stage packings, which are sensitive to adhesion levels, division times and division rules. In this scenario, a very tight control of division axis and timings would be necessary to ensure proper embryonic packings. While it would be possible to find a set of division rules and timing of divisions to encode virtually any blastomere packings, in this scenario the packing configurations would be highly sensitive to noise and not very robust. In embryos without a confining shell, or in meroblastic cleavage (zebrafish, etc.), the attachment of cells to the yolk may prevent slow rotational diffusion of blastomeres. In this case, the division rules are essential to control blastomere packing configurations [45].

Our results indicate that the presence of a confining shell removes degeneracies in the packing configurations and robustly established a stable configuration, solely dependent on the shape of the confining shell. For spherical shells, this leads to a unique tetrahedral packing, as observed in mouse embryos [46, 18, 23] and nematode worms [57, 21, 72] with spherical confinement. Our results also reproduce the observed packing configurations in different species of nematodes with varying degrees of shell elongation [57, 72], and

agrees well with previous models and experiments of this process [72]. We find that the role of the confining shell is to enforce a robust 4-cell stage packing configuration that is largely insensitive to noise in division times or division rules, as the cellular packing is independent of these parameters and depends only on the geometry of the shell. Moreover the presence of the shell decreases significantly the time for the blastomeres to reach the equilibrium configuration. In this scenario, division rules would control the packings only if blastomeres divide extraordinarily fast (< 0.1 min; $\tau_R \sim 1$ min [58]), before the blastomere packings set by the confining shell are established. This is an unlikely scenario because blastomeres do not divide at these rates. Essentially, the shape of the confining shell guides the cellular packings through development, ensuring that cell-cell contacts are made properly even in the presence of noise.

In the case of sticky confining shells, our work suggests that the robust square arrangement observed in echinoderms cannot be explained solely by the strong adhesion to a spherical shell (hyaline layer), as we the experimentally observed square blastomere arrangement was only obtained 50% of the times in the simulations. Observations of the hyaline layer in the early sea urchin embryo show that it closely surrounds the blastomeres and that it plastically deforms upon divisions. The precise shape of the hyaline layer and its temporal shape changes were not accounted for in our simulations and it is likely that they play an important role in determining the 4-cell stage blastomere packings.

A novel feature of this work is the use of 3D Voronoi tessellation to determine the topological blastomere arrangements (cell contact arrangement) in a particle-based de-

scription. Previous particle-based models of the early embryo that classified arrangements [72] employed distance measures to determine if two cells were in contact. We find that for high contact angles or for cells under strong confinement, this metric is not robust and can lead to erroneous contacts and unphysical dynamics. In the case of two cells dividing perpendicularly into four cells (ordered divisions), observed embryos would end up in a square configuration. For moderate contact angles, all four cells are within the contact distance and they all, incorrectly, feel attractive forces from the other three cells leading to quick relaxation to a tetrahedron. The 3D Voronoi tessellation allows to properly find the cells that are in contact and account for the proper forces acting on each cell. Using the Voronoi tesselation allows the adhesive square to persist and then to preferentially relax into a diamond configuration which then takes a long time to finally relax to a tetrahedron. In addition, using a distance metric for topology determination would fail to distinguish between four adhesive cells in a square or four cells in a tetrahedron whereas the 3D Voronoi tessellation separates these two distinct topologies. Therefore, using Voroni tessellation to properly determine cell contacts is essential to determine not only the packing configurations but also the dynamics of the blastomeres.

As in any particle-based model, our description does not account for the effect of changes in cell shape on the resulting force between cells or contacts, which may be relevant in some situations to accurately predict blastomere motions or the axis of cell divisions. Previous particle-based models have shown that it is possible to properly account for the dynamics of the blastomeres in early *C. elegans* embryos [16]. However,

it is unclear if in some cases where cell shape changes are different and more complex the particle-based models would still be accurate. In contrast to particle based models, other descriptions simulate the cells shapes to account for geometry-dependent division rules [45]. These descriptions rely on energy minimization (Surface Evolver [10]) to obtain cell shapes and are therefore limited to equilibrium packings. Our work combines the fast simulation power of particle description with Voronoi tessellation to determine cell neighbors, which is typically more accurately done in simulations accounting for cell shapes. We expect our description to fail if cell shapes are not compact (e.g., very elongated cells) because in these conditions the Voronoi tessellation would not provide a faithful representation of cell-cell contacts. Using this hybrid simulation method, we can explore the non-equilibrium dynamics of cellular packings that cannot be captured by equilibrium descriptions.

Our work demonstrates that physical confinement provides a powerful way of robustly guiding the blastomeres to one particular arrangement, strongly reducing the set of possible arrangements an embryo could take and helping guide the embryo developmental trajectory.

Chapter 3

Robustness of the *C. elegans* early embryo cellular arrangements to noise

3.1 Introduction

During early embryonic development, the correct arrangement of cells can be critical to proper further development because cell-cell interactions are necessary to establish downstream cell fates [19, 49, 67, 4, 48]. In particular, in nematodes, where cell positions and cell-cell contacts are highly stereotypical [51, 55, 14, 62], the early specification of cell identities due to their spatial arrangements is essential for the viability of the organism. For example, in *C. elegans* at the 4 cell stage (see Fig 3.1e), the fates of ABa and

ABp (which both express GLP-1/Notch) are not fully specified until one of them makes contact with P2 (expressing APX-1/Delta)[49, 48]. Reversal of the placements of P2 and EMS would lead to a non-viable embryo[48]. Furthermore, embryos that do not have the proper diamond arrangement at 4 cells will not hatch[72]. Embryos must therefore have mechanisms to robustly guide cells into the correct arrangements against sources of noise like division timing errors and division plane mis-specification[51, 5]. As embryos are physical systems, cell arrangements are ultimately dictated by the forces acting on cells in each embryo.

One major source of constraint is the envelope that surrounds the embryos of many species and in the case of nematodes is a hard chitinous eggshell[54, 21, 57, 72]. Recent work has shown that the geometry and volume of the eggshell puts strong constraints on the arrangements of cells that can exist inside and that there is often only one dominant arrangement topology that can exist for a specific shell aspect ratio (like the diamond arrangement in wildtype *C. elegans*)[72]. Other work has shown that removing the eggshell can lead to incorrect arrangements in early *C. elegans* embryos which are eventually lethal[17]. However, even if only the 4-cell diamond topology is possible, there are 6 possible distributions of cell identities within the diamond topology with several (like reversal of P1 and EMS) being lethal. How does *C. elegans* robustly guide early development to the proper cell distributions and avoid the lethal ones?

In wildtype *C. elegans*, the timing and orientation of cell divisions are tightly controlled. Although the overall timescale between embryos can change due to embryo

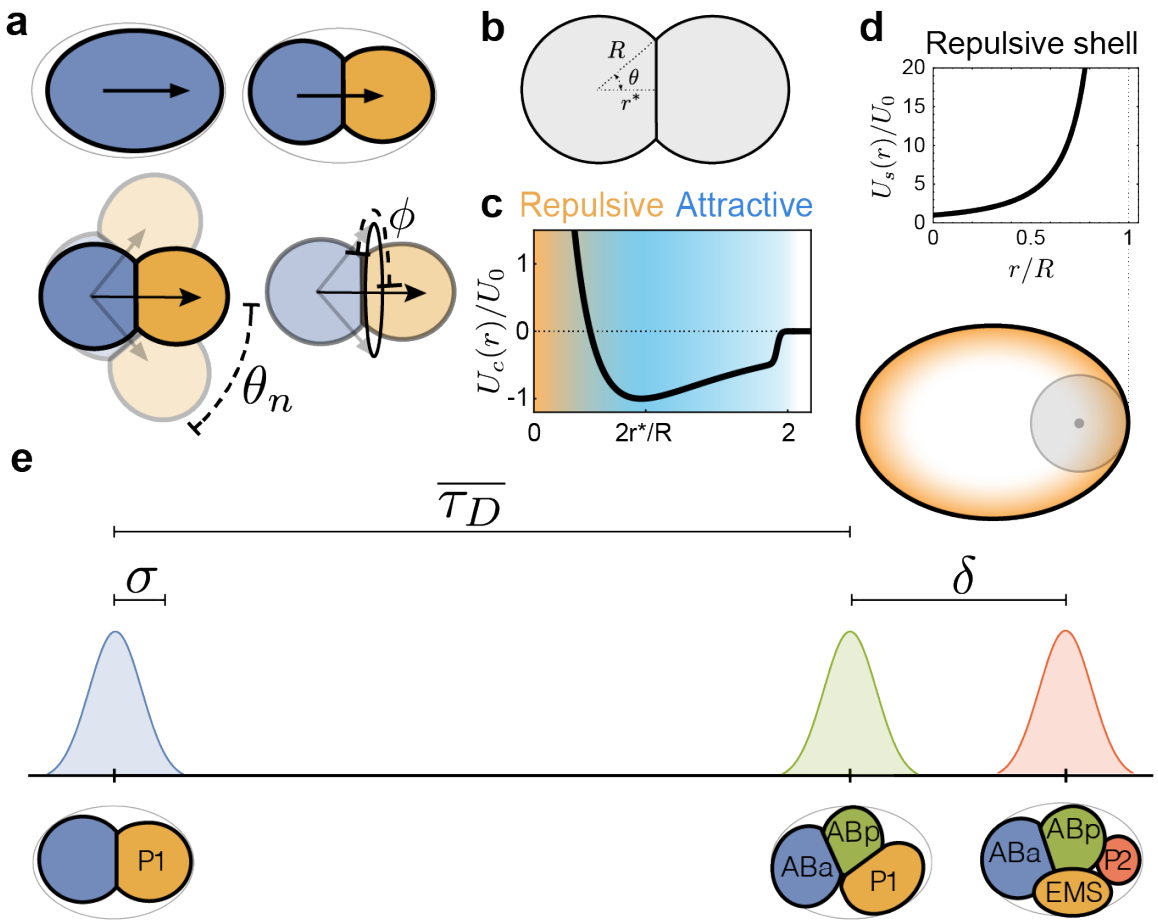

Figure 3.1: **Simulating the early *C. elegans* embryo** A: Diagram of a division with no noise, division with angular division noise θ_n and the possible ring of divisions from a uniformly distributed ϕ angle. B: Abstraction of cells to central points with contact size R, equilibrium distance $2r^*$ and contact angle θ. C: The radial potential between two cells has a cutoff distance at $2R$, an attractive region from $2R$ to $2r^*$ and a repulsive region within a distance of $2r^*$. The minimum of the potential is normalized to -1. D: A contour diagram of the repulsive potential used for the confining shell with orange values being greater than blue values. (Here the shell has an aspect ratio of 1.) The inset shows the radial one-dimensional form of this potential which diverges at the shell. E: Schematic of the first three divisions of the wildtype *C. elegans* embryo. The first division along the anterior-posterior (AP) axis leads to two unequal blastomeres named AB and P1. AB divides first perpendicularly to the AP axis resulting in the ABa and ABp daughter cells. P1 asymmetrically divides soon after along the AP axis resulting in the EMS and P2 cells. Notch/Delta signalling occurs by contact between the ABp and P2 cells. The thin gray outline represents the chitinous eggshell surrounding the embryo. The average time between all divisions (except P1) is $\overline{\tau}_D$. The timing noise added to each cell is Gaussian noise with standard deviation $\sigma\overline{\tau}_D$. The relative offset between the AB and P1 divisions is δ.

variability and temperature, Bao (2008)[5] found that the variability of the relative time differences between divisions had a standard deviation of only 7% for the first 8 divisions. Richards (2013)[51] quantitatively tracked cell trajectories for the full duration of development and also found conserved division timings and deviations between embryos of on average about $27^\circ \pm 5^\circ$ for division angles. It has been observed that increases in variability or strong changes in timing or division orientation strongly decrease the hatching rate[51]. However, the precise effect of such noise on proper cell arrangements has not been systematically studied.

Here we use a 3D Voronoi-augmented Langevin simulator to study the robustness of four cell arrangements in *C. elegans* to noise in timings and division angles, to changes in the mean timings between the AB and P1 divisions, and to the deterministic varying of the AB and P1 division angles. We find that the early embryo is completely robust to moderate levels of timing noise and division angle noise and further subdivide lethal errors at higher noise levels into placement errors or timing sequence errors where one cell lineage divides much quicker than the other. We also study the effect of changing the timing offset between AB and P1 and find that its main effect for moderate changes is to cause a non-lethal ABa-ABp switch. Finally, we vary the division angles of AB and P1 independently and determine the final arrangement for each angular pair. We find that due to the constraints of the egg shell, the cell arrangements at three cells neatly split at an angle of 90 degrees and the arrangements of four cells mostly follow this pattern as well with P1 division angles above 90° usually leading to a lethal configuration. Overall, our

results demonstrate how confinement, division timing and division rules all contribute to ensuring robust development with confinement setting the overall shape (a diamond) and division timings and rules specifying where individual cells will go within that shape.

3.2 Methods

Numerical Simulation

The 3D Langevin equations (Eq. 3.6) governing the motion of cells were solved via the Euler-Maruyama method [28]. Simulations were run using a timestep $\Delta t \equiv 10^{-3}\tau_R$, much smaller than all relevant timescales in the system, namely τ_R and τ_D. The discretized version of Eq. 3.6 integrated numerically reads

$$\vec{r}_i(t+\Delta t) = \vec{r}_i(t) - \sum_{j\in\Omega_i^t} \partial_{r_{ij}} \tilde{U}(r_{ij};\,\theta)\,\Delta t + \sqrt{2\sigma\Delta t}\,\vec{\eta}\,, \tag{3.1}$$

where θ are the cell-cell potential parameters (Methods), σ is the random noise scale (set to 5×10^{-5}), $\vec{\eta}$ is a standard normal random vector with each component drawn from $\mathcal{N}(0,1)$ and Ω_i^t is the set of cells in direct contact with cell i at time t. The elements of the set Ω_i^t are obtained from the Voronoi tessellation of the system at time t (Methods).

Simulations were initialized with the undivided egg (first cell) placed in Gaussian distributed initial positions with variance $b/10$ around the origin. Simulations ended the timestep before a cell division would change the total number of cells to be above 4.

Cell-cell interaction potential

The cell-cell interaction potential has a Lennard-Jones like form, but is multiplied by a support function that cuts it off at a given distance while keeping it continuous and differentiable (Fig 3.1c). The cutoff distance for a given cell pair i and j is set to $R_i + R_j \equiv R_{ij}$, with R_i and R_j being the radii of cells i and j, respectively. The size of each cell (or the radius equivalently) can be different because of the volume conservation correction and because of cell divisions (see Methods below). The potential has an equilibrium distance $r_i^* + r_j^* \equiv r_{ij}^*$ (Fig 3.1b) which is the equilibrium distance between two cells combining the equilibrium radii of each cell. The form of the cell-cell potential is

$$U(r_{ij}; r_{ij}^*, R_{ij}) = \frac{U_0}{(\alpha - \beta)} \left[\frac{1}{1 + f(r_{ij})} \right] \times \left[\frac{(r_{ij}^*)^\alpha (\beta + f(r_{ij}^*) \left[\beta + \frac{r_{ij}^*}{\tilde{a}} \right])}{r_{ij}^\alpha} - \frac{(r_{ij}^*)^\beta (\alpha + f(r_{ij}^*) \left[\alpha + \frac{r_{ij}^*}{\tilde{a}} \right])}{r_{ij}^\beta} \right], \quad (3.2)$$

where the α, β, and a are parameters characterizing the shape of the potential and the cutoff support function, U_0 is the energy scale of the potential (the potential equals -U_0 at its minimum) and $f(r_{ij}) \equiv e^{\frac{(r_{ij} - R_{ij})}{a}}$. We set $\alpha = 4$, $\beta = 3$, and $\tilde{a} = 0.01$.

Confining Shell

The shape of an axisymmetric ellipsoidal shell, and the associated ellipsoidal level set, are given implicitly by

$$\frac{x^2}{a^2} + \frac{y^2}{b^2} + \frac{z^2}{b^2} = c\,, \tag{3.3}$$

where a is the length of the ellipsoid's major axis, b is the length of its minor axis and$c$ is a positive constant that defines the ellipsoidal level set where $c = 1$ defines the shell itself.

Since cells cannot penetrate the shell, the confining potential must diverge at the positions where the shell is located ($c = 1$). Moreover, the potential must vanish when the cell can no longer be in contact with the shell, which occurs when a cell is located at a distance larger than R from the shell. With this in mind, we define the confining potential of a repulsive shell U_{rs} (Fig 3.1d) as

$$U_{rs}(x, y, z; R, k_{shell}) = \frac{k_{shell}}{1 - \sqrt{\frac{x^2}{a^2} + \frac{y^2}{b^2} + \frac{z^2}{b^2}}}\,\Theta\left(\sqrt{\frac{x^2}{a^2} + \frac{y^2}{b^2} + \frac{z^2}{b^2}} - (1 - \frac{R}{b})\right) \tag{3.4}$$

where k_{shell} is the energy scale of the shell potential and $\Theta()$ is the Heaviside step function that sets the function to zero when a cell is too far from the shell to be in contact. We used a Heaviside step function instead of using a support function to cut off the potential above cell size for mathematical convenience.

We set $k_{shell} = 10$ to balance the repulsion forces between two cells and between cells

and the shell when in steady state confinement.

The force acting on cell i arising from contact with the shell is given by

$$\vec{F}_i^s = -\nabla U_{rs}(\vec{r}_i)\,, \tag{3.5}$$

where $\vec{r}_i$ is the position of cell i.

Topology Inference

Because we simulated particles in a confined volume, it was necessary to move beyond a simple distance metric to determine if two cells were neighbors. We use a 3D Voronoi partitioning as an extra constraint in addition to distances. The package we used, Voro++[52], determines the 3D Voronoi polytope around each cell by starting with a large 3D volume and then cutting it using the midplanes from the current cell to each of its neighbors. In this work, each cell starts with a dodecahedral volume that surrounds an inscribed sphere with the cell radius R. When a pair of cells are close enough, their dodecahedral volumes are cut by the weighted midplane between them (adjusted from the midpoint by their respective radii) (Fig. 2.1g). Each new cut face of the Voronoi polytope is identified with a neighboring cell allowing all neighbors to be identified. Using a 3D Voronoi partition is critical to properly detect when cells are not in contact even when they are within the contact distance due to blocking by neighboring cells. It was also necessary to have the square arrangement of cells be distinguishable from the tetrahedron since with soft spheres, both cases have all cells within the contact distances

of all others. Finally, using the 3D Voronoi to determine neighbors is critical to avoid soft spheres unphysically always forming a tetrahedron when strongly confined.

Two cells are defined to be in contact when they are within R_{ij} of each other and their Voronoi polytopes share a face. An adjacency graph is created by defining each cell as a node and adding edges between each pair of cells found to be in contact.

Adjacency matrix timing correction

The wildtype adjacency matrix at 4 cells has ABa at node 1, ABp at node 3, EMS at node 2 and P2 at node 4. In the simulator, cell numbering is given based on cell division order. For wildtype, these numbers correspond with the wildtype numbering. However, if P1 divides before AB, the numbering for ABp and P2 get reversed. We relabel these two cells by detecting if P1 divides before AB and if so apply permutation matrices to transform the adjacency matrix.

Error topology detection

We check whether the simulation adjacency matrix at the last timestep equals adjacency matrices for each of the 6 possible configurations that the shell diamond constraint allow.

Cell divisions

Each cell i has a timer that decrements every timestep. For all cells except P1, the timer's length is $\overline{\tau_D} \pm$ the relative noise imposed. For P1, it is $(1+\delta)\overline{\tau_D}$ plus noise. When this

timer runs out, the cell divides according to the division rules below and each daughter cell's timer is reset.

When a cell division occurs, all lengths associated with cell i are scaled down by $2^{1/3}$ to decrease the volume of the cell by half. A new cell is placed a distance R_i away from the parent cell center. (except for the deterministic divisions in the last section where the new cell was placed $.5R_i$ away).

With no noise, the axis of division follows the wildtype T division rule. The first division from one cell to two (AB and P1) occurs along the x-axis. The AB division occurs along the y-axis while the P1 division again occurs along the x-axis.

Noise is added to the division axis by changing the θ angle of the division axis by an exponentially distributed angle with a specified mean $\overline{\theta_n}$ and with a uniformly distributed ϕ angle.

For the deterministic divisions, all cell divisions were along the x axis and the division axis θ angle was systematically adjusted while again having the ϕ angle be uniformly distributed creating a cone of possible division axes. This was chosen due to the ϕ symmetry of the egg shell.

Volume Adjustment

The overlap between blastomeres was determined by defining a sphere with radius R_i around each cell i and then calculating its overlap volume V_o with neighboring spheres. This overlapping volume is added to cell i, making its size larger. In particular, the

radius of cell i is modified from R_i before the correction to R_i' after it, with $4\pi(R_i')^3/3 = 4\pi(R_i)^3/3 + V_o$ (Fig 2.1e). This adjustment is performed once per timestep. The Voronoi dodecahedron is also scaled to surround a sphere of radius R_i' after volume correction.

Spline approximation for plots

We used Mathematica's BSplineFunction [69] to fit a non-uniform rational B-Spline surface to the simulated noise data. We used a degree of 30 to smooth the variance in the data and to extract the mean surface for generating contour plots.

Percent determination for errors

We determined the percent of errors arising from different deterministic division angles by summing the number of simulations in each of the four quadrants of the plot and dividing this number by the total number of simulations.

3.3 Results

Theoretical Description

To simulate the 3D dynamics of blastomeres, accounting for cell-cell interactions, cell divisions and embryo confinement, we use a minimal representation and describe each blastomere (cell) as a particle. Particle-based descriptions have previously been used to describe blastomere motion in early *C. elegans* embryos and shown to properly describe

cellular movements [15, 16, 72]. In this particle-based model, the mechanical interaction between cells is represented by an interaction potential $U(r_{ij})$ that effectively accounts for (adhesion, etc. [44]), where $r_{ij} = |\vec{r}_i - \vec{r}_j|$ is the distance between two given cells located at positions $\vec{r}_i$ and $\vec{r}_j$. Cell-cell adhesion is represented by an attractive range in the potential, whereas a repulsive region ensures that cells do not interpenetrate when they come too close to each other (Fig. 3.1b). To account for cell size in this particle description, we include a sharp cut-off of the potential at a distance R, which corresponds to the radius of an isolated blastomere. The balance of attractive and repulsive forces between two blastomeres occurs when they are separated by a distance $2r^*$. The ratio between this equilibrium distance between blastomeres and the blastomere size $2R$ corresponds to $r^*/R = \cos\theta_c$, with θ_c being the contact angle between cells (Fig. 2.1c,d). Since the contact angle is an easily measurable quantity that informs about the relative strength of adhesion and cortical tension [35, 72], we use θ_c as control parameter instead of r^* and choose $\theta_c = 46°$ which is similar to contact angles observed in early *C. elegans* embryos[72]. Moreover, although it is not possible to enforce exact volume conservation in a particle-based description, we perform leading order corrections upon cell contact (Fig. 2.1e; Methods); we have checked that the volume corrections are small and we have tested that our results do not qualitatively depend on them.

At the spatial and temporal scales of embryo development, the system is overdamped and inertia can be safely neglected [50]. Therefore, force balance (momentum conserva-

tion) for a given blastomere reads

$$\mu \frac{d\vec{r}_i}{dt} = \sum_{j \neq i} \vec{F}^c_{ij} + \vec{F}^s_i + \vec{\eta}_i \,, \tag{3.6}$$

where $\vec{r}_i$ is the position of cell i in 3D, $\vec{F}^c_{ij} = -\nabla U(r_{ij})$ are the forces that cells in contact apply on each other, $\vec{F}^s_i$ represents the force of a confining shell on cell i (whenever a confining shell is present), and $\vec{\eta}_i$ is a small fluctuating force (Gaussian white noise) that represents the force fluctuations acting on each cell. Finally, the parameter μ corresponds to a friction coefficient that resists cell movement in an overdamped environment and it is here assumed constant and equal for all blastomeres. To obtain the force $\vec{F}^s_i$ from the confining shell on cell i, we define the geometry of the confining shell and set the interaction potential $U_{\text{shell}}(x, y, z)$ that a cell would perceive inside the shell (Fig. 3.1d; Methods). The confinement force encountered by cell i is then given by $\vec{F}^s_i = -\nabla U_{\text{shell}}(x, y, z)$ (Methods).

To properly determine which cells are in contact and can therefore apply forces on each other, we use Voronoi tessellation (Methods; Fig. 2.1i). Previous particle-based simulations have use distance-based metrics to determine the neighbors of each cell. However, distance-based metrics give erroneous results for both cell-cell contacts and dynamics in the presence of confining shells. When cells are strongly confined, the distance between next-nearest neighbors can be smaller than the interaction potential range, leading the simulation to erroneously include the forces of cells that are not in direct contact. Voronoi tessellation overcomes this problem and the enables proper determination of

cell-cell contact topology at each timestep of the simulation (Methods).

We approximate the shell surrounding the *C. elegans* embryo by an axisymmetric ellipsoid with major and minor axes a and b, respectively, with volume $V_s = \frac{4\pi}{3}ab^2$ and an aspect ratio $a/b = 1.6$ which is the mean observed aspect ratio for wildtype *C. elegans*[72] and a volume ratio between the shell interior and the initial egg cell (V_s/V_c) of 1.2. Since blastomeres cannot penetrate the shell, we used confining potential forms that diverge at the shell boundary (Methods; Fig. 3.1d). Moreover, the confining potential vanishes for distances larger than R from the shell, as these are not within the reach of cells.

Beyond physical interactions among cells and with the confining shell, blastomeres in early embryos divide at regular intervals, with a time $\overline{\tau_D}$ between division events (Fig. 3.1e). In wildtype *C. elegans*, the P1 cell divides after the AB cell divides. This leads to $\overline{\tau_{P1}} = (1+\delta)\overline{\tau_D}$ where δ is the relative time difference between when the AB and P1 blastomeres divide. In wildtype embryos, $\delta \sim 10\%$[11, 5]. To introduce noise into the division times, each cell was given an individual division time generated by perturbing the mean division time $\overline{\tau_D}$ with Gaussian noise with a standard deviation $\sigma\,\overline{\tau_D}$ where σ is the relative amount of noise being considered (except for the P1 cell, which has a mean of $\overline{\tau_{P1}}$ instead).

Simulated division events (Methods) correctly change the volume of daughter cells upon division. For symmetric divisions (the only type considered here), the volume of the daughter cells is half of cell volume before division, and so the cell radius R

changes after each division cycle to $R_n = R_0/2^{n/3}$, where R_0 is the radius of the initial egg (and $V_c = 4\pi {R_0}^3/3$ is the initial egg volume) and n is the number of divisions that have occurred (Fig. 2.1h). Finally, in order to study the role of division rules, we control the spatial direction along which the division occurs (perpendicular to the mitotic plane [41, 20]). In wildtype *C. elegans*, the fertilized egg divides along the anterior-posterior (AP) axis to form the AB and P1 cells. Then the AB cell divides perpendicular to the AP axis and finally the P1 cell divides along the AP axis following a T-shaped division rule[72, 29, 17]. Noise was added to these divisions by perturbing the division axis an amount θ_n selected from an exponential distribution with mean $\overline{\theta_n}$ and a uniformly random ϕ_n forming a cone around the unperturbed division axis (Fig. 3.1a).

To systematically study the deterministic effect of division rules, we also studied the arrangements that result by varying the division axis angles of AB and P1 with no noise present. Unlike in the wildtype case where the division rule is T-shaped, the division axis direction for $\theta = 0$ is defined to be along the AP axis facing the anterior for both AB and P1 divisions. A uniformly random ϕ is still applied creating a division axis cone with a cone angle of θ around the AP axis.

Normalizing all lengths by the initial egg radius R_0, all forces with U_0/R_0 and time with the mechanical relaxation time τ_M, which is given by $\tau_M \equiv \mu R_0^2/U_0$ and represents the characteristic timescale over which mechanical disturbances typically relax to equilibrium, the relevant dimensionless parameters in the problem are δ, ϵ, $\overline{\theta_n}$ with several of the dimensionless parameters set to constants: $\tau_D/\tau_M = 10$, $a/b = 1.6$, $V_s/V_c = 1.2$, and

$\theta_c = 46°$.

Dimensionless Parameters	
Parameter	Description
δ	*Relative offset between P1 and AB division times*: Specifies the relative time increase of the mean P1 division compared with the AB division time
σ	*Relative strength of timing noise*: The standard deviation of the Gaussian perturbation around the mean division time is $\sigma\ \tau_{AB/P1}$
$\overline{\theta_n}$	*Mean value of division angle noise*: Angular deviations from the wildtype division rule are chosen from an exponential distribution with a mean of $\overline{\theta_n}$

Table 3.1: Definition of the relevant dimensionless parameters in the problem.

In what follows, we simulate the stochastic movements of the multiple interacting blastomeres using Langevin dynamics (Eq. 3.6; Methods) in different conditions.

Wildtype embryo robustness to timing noise and division angle noise

At the 4 cell stage in *C. elegans*, the proper placement of each cell in the diamond packing topology is necessary to ensure the correct cell-cell contacts. Since errors in the placement of cells within the diamond topology will depend on changes to cell division timings and division angles, we studied how increasing variability to timing and angles would lead to lethal arrangements.

In our simulator, every cell has a unique identity that is consistent between simulations and allows changes in cell positioning to be easily determined. Consistent labeling is

necessary to describe, for example, a reversal of the positions of the ABa and ABp cells from their wildtype configuration. Even though ABa is anterior to ABp in wildtype, it is possible for ABp to end up anterior to ABa if their positions are reversed. Our labels (ABa, ABp, P1 and EMS) indicate the identity that each blastomere would have following wildtype division timings and division rules without noise. Furthermore, because the ABa and ABp blastomeres are equivalent before further interaction with the P1 blastomere, we consider the switching of the wildtype ABa and ABp to be nonlethal. However, the simulator can still determine when an ABa-ABp reversal has occurred.

Using a wildtype-like timing offset of 10% between when AB and P1 divide and the standard T division rule, we varied the strength of noise in the timing of divisions from 0% to 50% and noise in the angle of each cell's division axis from no error to a mean error of 90°.

We find a region of zero lethal errors with timing noise below 27% and division angle errors below a mean of 27° (Fig 3.2a). The naturally reported variability in *C. elegans* was observed to be $\sim 7\%$ for division timings and $\sim 27°$ for division angles [51] (although this amount of angular noise is likely an overestimate for the very early embryo). This natural variability occurs within this region of zero errors which matches the observation that wildtype embryos have a 95-99% hatching rate[71, 65, 7]. Above these noise thresholds, rates of lethal misplacements additively increase.

To investigate the root cause of these lethal errors, we subdivided these errors (Fig 3.2a) into lethal placement errors (cells ended up in a non-wildtype position and contact

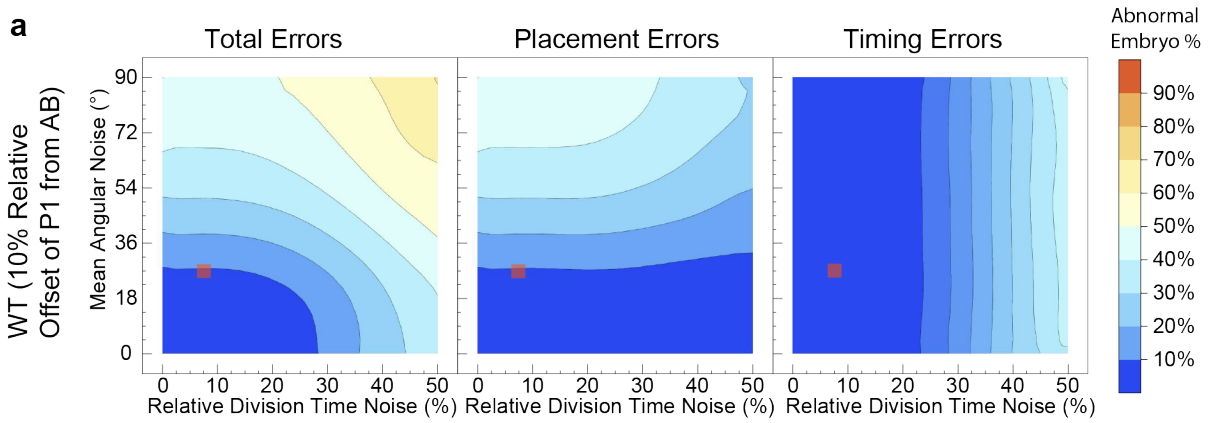

Figure 3.2: **Simulations of wildtype robustness.** A: Contour plot of the percentage of lethal errors for various levels of timing noise and angular noise for an embryo with wildtype division rules and timing offset. The lethal errors can be subdivided into placement errors (cells in non-wildtype place in arrangement) and timing errors (one cell lineage has divided twice before the other has divided once). Using a wildtype-like timing offset of 10% between when AB and P1 divide and the standard T division rule, 500 simulations were run for each parameter value varying the amount timing noise from 0-50% in increments of 2.5% and the angle noise from 0-90 degrees in increments of 4.5 degrees. Red square denotes the observed variability in wildtype of 7% standard deviation of relative timings and $\sim 27^\circ$ of angular noise.

arrangement other than ABa-ABp reversal) or division timing errors (one cell had divided twice before another could divide once). Lethal placement errors mostly depend on increasing angular noise but are less sensitive to increasing division noise meaning that the lethal configurations where EMS and P2 are reversed require a sizeable amount of noise to occur. The other type of error only depends on timing noise and occurs when either AB or P1 divide twice before the other blastomere can divide once, leading to a generation sequence out of sync with the expected wildtype sequence. This requires overcoming a certain threshold of timing noise that can occasionally push the cell division time far enough away from the mean division time to cause the timing error to occur.

Embryo robustness to timing noise and timing offset between divisions

The relative timing offset between the AB and P1 divisions in *C. elegans* in wildtype embryos is robust and is maintained through a wide temperature range [51]. To investigate the effect of varying the timing offset between the AB division and P1 division from its relative 10% difference in wild-type embryos[5, 30], we varied the relative offset δ from -70% to 70%. To further study the interplay between the timing offset and the embryo's robustness to noise sources, we also varied the division timing noise from 0% to 50% with three different levels of division angle noise: $0°, 18°, 54°$.

Overall, the error rate looks to be symmetric around an offset of $\delta = 0$ with the onset of lethal errors occuring for lower values of division noise as the timing offset increases (Fig 3.3a). There does not seem to be a strong effect from division angle noise values below the 27° zero error threshold found in Fig 3.2c, but for the division noise value of 54°, the error rate in the low noise/low offset regime increased from 0% to 40%.

What is the effect of changing the timing offset δ if it does not lead to lethal errors? Fig 3.3b focuses on the frequency of the non-lethal ABa-ABp reversal to occur. Decreasing the relative timing offset leads to up to a 30% frequency of ABa-ABp reversal. Increasing the division angle noise to 18° leads to some non-lethal ABa-ABp reversal occurring even for an increased timing offset. Having a much higher division angle noise value causes many more lethal errors and decreases the occurrence of nonlethal reversals.

By focusing only on lethal errors that came from timing sequencing errors (Fig 3.3c),

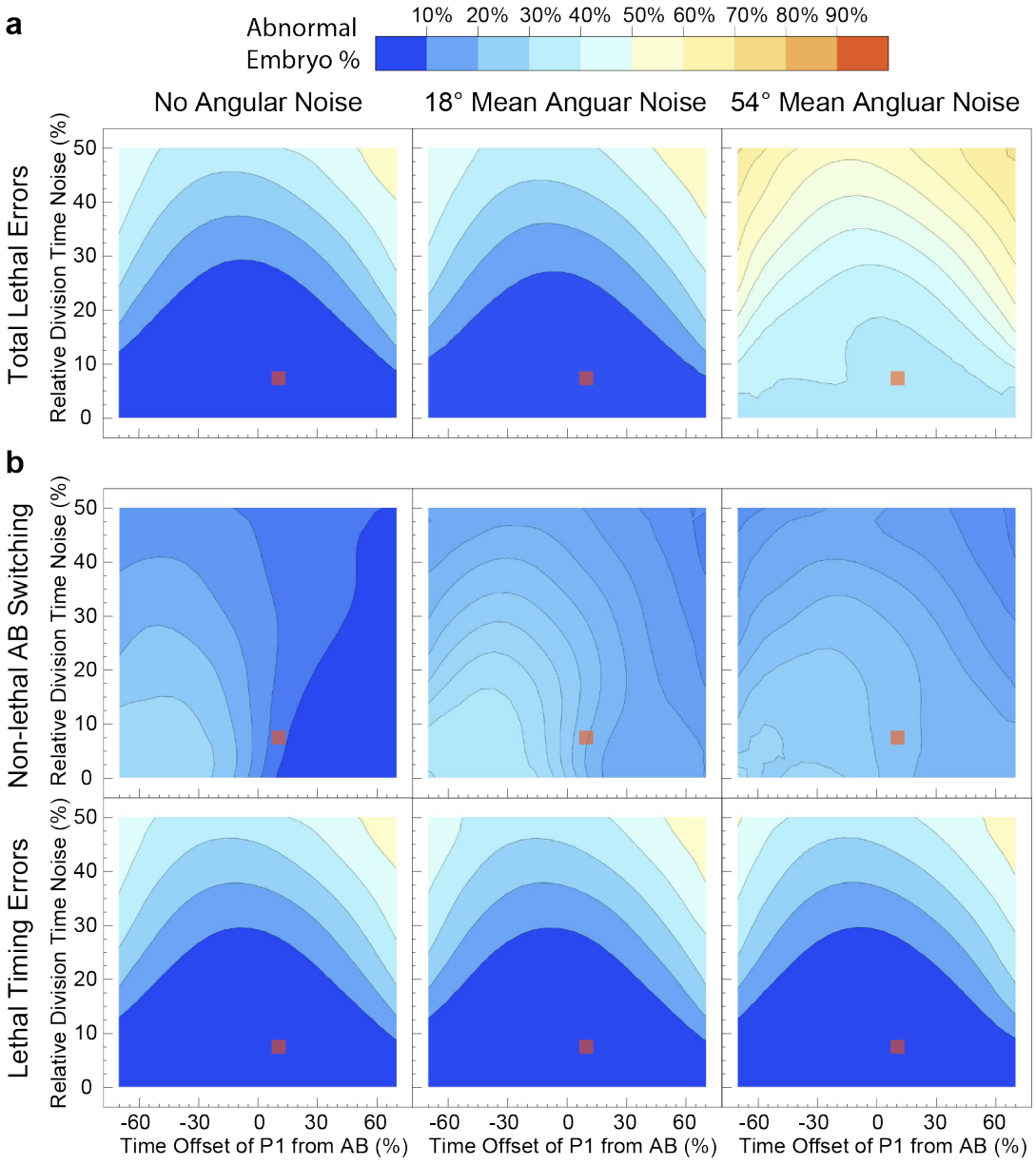

Figure 3.3: **Simulations of robustness to timing noise and timing offsets.** A: Plots of percentage of lethal errors varying timing offsets and timing noise for three angular noises. 500 simulations were run per parameter and varying the offset between AB and P1 from -70% to 70% of the average cell division time τ_D in 5% increments and varying the division timing noise from 0% to 50% in 2.5% increments. The wildtype T division rule was used and the division angle noise was held constant at 0, a mean of 18 degrees and a mean of 54 degrees. Red square denotes the observed variability in wildtype of 7% standard deviation of relative timings and a relative offset $\delta \sim 10\%$. B: (top) Percentage of non-lethal AB Switching error (bottom) Percentage of division timing errors (cells more than two divisions out of sync).

we see that for low values of division angle noise, the only lethal errors are timing sequencing errors and that this pattern is not changed for high division angle noise which means that the increased lethal errors must be cell placement errors. As was found earlier, division angle noise increases placement errors and division timing noise leads to timing sequence errors. The effect of changing the relative timing offset δ increases the embryo's susceptibility to timing sequence errors and decreasing the timing offset leads to more non-lethal ABa-ABp reversals.

Embryo robustness to deterministic variation of division rules

What final arrangements do different division rules lead to in the early *C. elegans* embryo? To determine the effect of different division rules on the resulting arrangement, we systematically varied the angle of division for both AB and P1 with no division angle noise, no timing noise and a wild-type timing offset of 10% between AB and P1. $\theta = 0^\circ$ is defined as dividing along the AP axis towards the anterior and the angle above 0° leads to the division occurring on a cone of that angle around the AP axis (since the angle ϕ around the AP axis is randomly sampled). We uniformly sampled division angles for the AB division (called θ_{AB}) from 0° to 180° and similarly for the P1 division (denoted θ_{P1}).

In Figure 3.4, we show the probability flow of arrangements of two cells to three cell configurations and then to the probabilities and division angles that lead to the final four cell arrangements with the wildtype arrangement and non-lethal ABa-ABp arrangement (in green) and the two lethal error arrangements (in red).

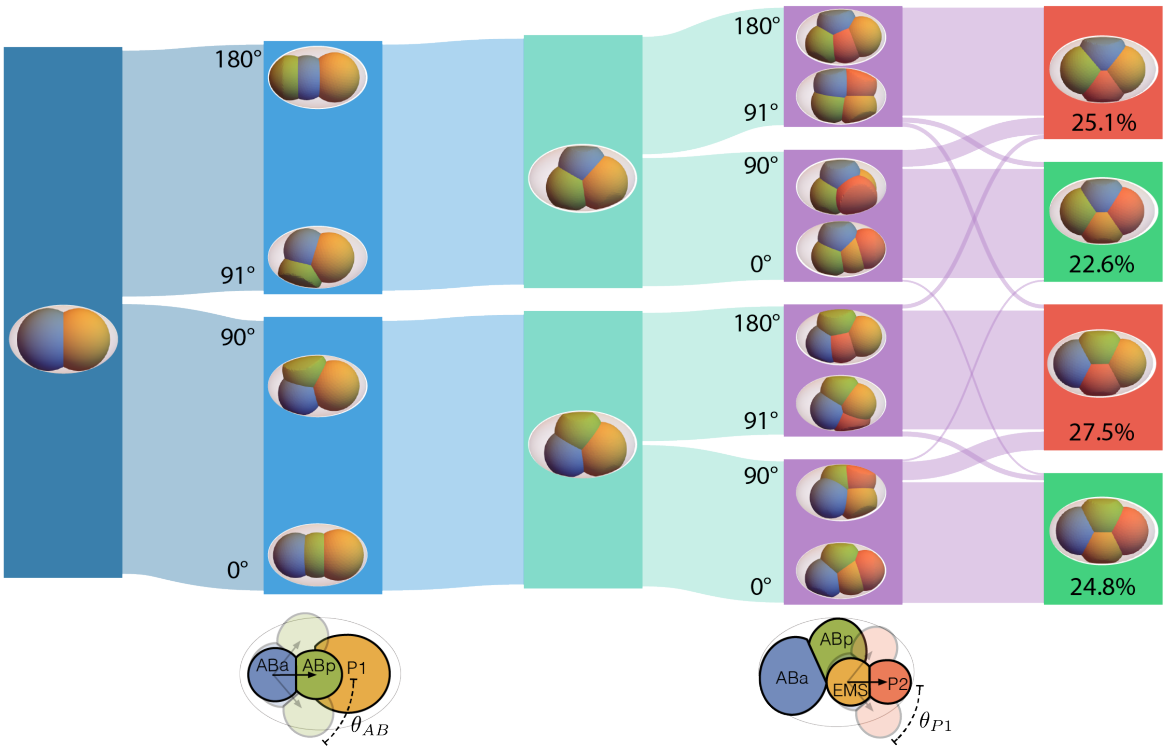

Figure 3.4: **Probability flow of arrangements from deterministic division rules.** A Sankey diagram showing the flow of probability for each type of arrangement to occur given a uniform sampling of division angles for AB and P1. We independently varied the division angle from 0-180 degrees in 9 degree increments for AB and P1 and ran 500 simulations for each angle value. AB division is shown in second column with the division angle varied between 0° and 180°. The second column shows the percentage of all simulations where the AB division was below or above 90°. The third column shows the two observed relaxed 3 cell states. The fourth column shows the percentage of simulations with a P1 division below or above 90° and the final column shows the percentages to observe each of the four final cell configurations with nonlethal configurations in green lethal ones in red. (Bottom) These two figures illustrate θ_{AB} and θ_{P1}.

Tracing the flow of observed final configurations backwards to the original two cells, we find that the probability flow splits evenly between angles below and above 90 degrees. Because of the shell confinement, division timing offset and the size asymmetry between P1 and the AB daughter cells, there are only two stable triangular cell arrangements with one coming from divisions below 90 degrees and the other form divisions above.

The timing offset in divisions between AB and P1 allows the three cells to relax to one of these two equilibrium configurations allowing for a diverse set of possible division angles to be robustly driven to just two possible arrangements. After the P1 blastomere divides, each stable three cell configuration splits into two paths for P1 divisions below and above 90 degrees.

Each final 4 cell state has a dominant contribution from a particular range of division angles. Starting first with the wildtype final arrangement (Fig 3.4, bottom right, in green), having the AB division less than 90 degrees leads to ABp (green) being between ABa (blue) and P1 (yellow). We see that both dominant final arrangements coming from this bottom half of the flow have ABp (green) in the middle and ABa (blue) towards the shell end. ABa and ABp are reversed for the top two arrangements where the AB division was greater than 90 degrees.

The same idea holds for the P1 division but is occasionally modified by the influence of the shell constraint on a particular range of division angles. Again, the dominant effect of P1 dividing below (above) 90 degrees is to place EMS (yellow) anteriorly (posteriorly). We see that the dominant path to the 4 cell wildtype arrangement with ABp and EMS in the center of the arrangement comes from both the AB and P1 divisions being below 90 degrees. Switching just the P1 division to be above 90 degrees usually leads to EMS and P1 (yellow and red) reversing places. Changing just the AB division above 90 degrees usually leads to ABa and ABp (blue and green) reversing places. And changing both division angles above 90 degrees leads to ABa and P1 (blue and red) switching to the

middle of the arrangement.

To understand the origin of the small streams of probability that do not follow the dominant flows of probability, we looked at the probability for all 4 final arrangements for each angle for both the AB and P1 divisions (Fig 3.5). This could not be deduced from the probability flow diagram in Figure 3.4 because the position of the stream's origin and destination does not encode extra information about its angle other than whether it is greater or less than 90°.

On all four plots in Fig 3.5, we see two important patterns. Most noticeably, we see each plot has a quadrant of high probability with steep sides perpendicular to the AB axis and a gentle upwards slope perpendicular to the P1 axis. We also see each plot has a faint horizontal line that goes out of the quadrant and has about a 10% difference from the surrounding probability (lower within the quadrant and higher outside).

The smooth ramp is what leads to the largest non-dominant flows into error 1 and error 3 configurations. Although changing the AB division angle through 90 degrees (while in the 100% part of the quadrant) leads to a sharp transition between 100% and 0%, changing P1 through 90 degrees causes a much more gradual transition from 100% to 0% which leads to some percentage of simulations with P1 less than 90 degrees transiting to the other state.

The horizontal line occurs right in the middle of the quadrant (e.g centered at 45 degrees for the wildtype quadrant) and represents a shift of some probability from the dominant final arrangement to the arrangement with reversed ABa-ABp cells. This shift

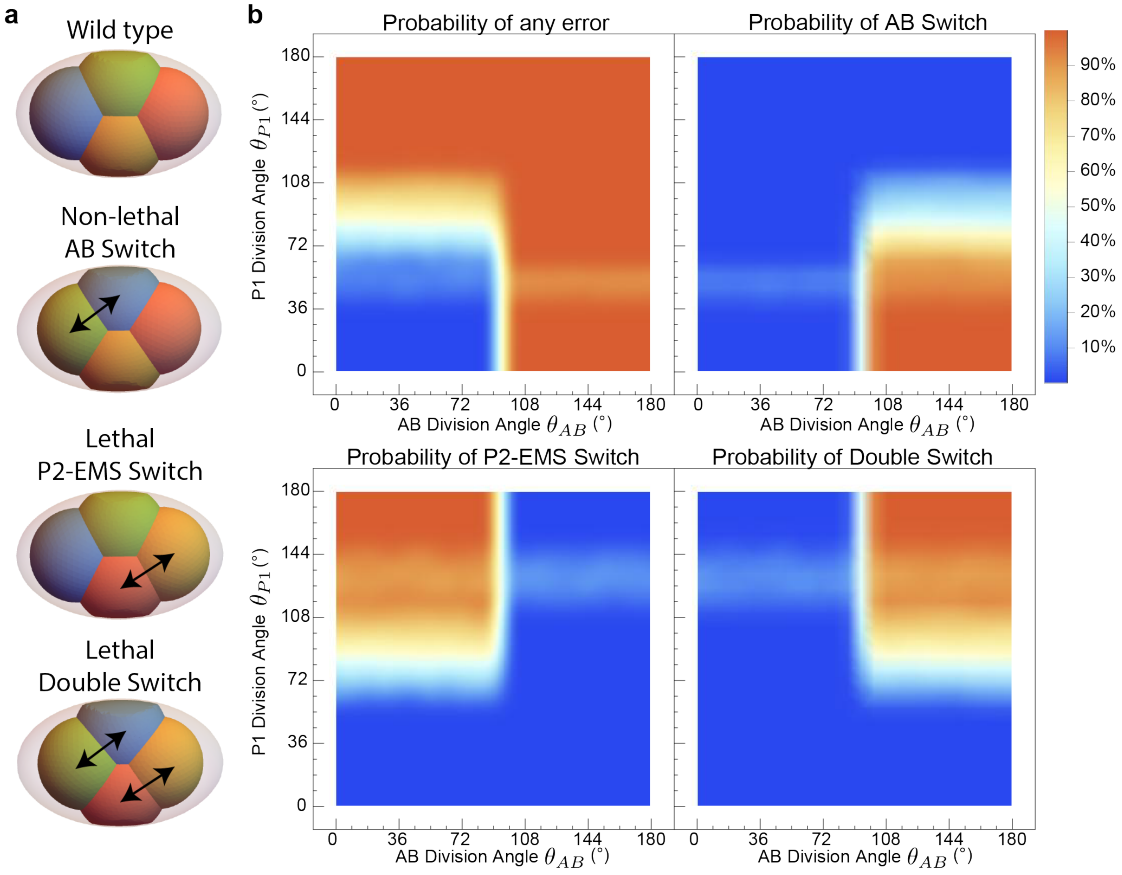

Figure 3.5: **Density plots of final arrangements for specific θ_{AB} and θ_{P1} values** A: Illustration of the cell placement error for each error type. B: Division angles were independently varied from 0-180 degrees in 9 degree increments for AB and P1 and 500 simulations were run for each angle value. (Top left) Density plot of the frequency of observing any non-wildtype arrangement for each pair of θ_{AB} and θ_{P1} values. (Top right) Density plot of the frequency of observing a non-lethal AB switch. (Bottom left) Density plot of the frequency of observing a lethal P1-EMS switch. (Bottom right) Density plot of the frequency of observing a lethal double switch. Note in all four density plots the faint horizontal line. This corresponds to a rare opposite rotation caused by a specific θ_{P1} and ϕ value.

occurs when the P1 cell divides in a very specific direction (in both θ and ϕ) causing the other three cells to be rotated so that the ABa-ABp positions are reversed. Because of the random ϕ division angle that is still present in these simulations, this only occurs for around 10% of the simulations in the small range of P1 division angle values. Since the

width of this horizontal feature is small, a 10% drop within the feature causes a much smaller total change of probability as reflected in the diagram.

3.4 Discussion

Here, we used a particle-based Langevin model to study the robustness of cell arrangements in the 4-cell *C. elegans* embryo. First, we investigated the effect of timing and division angle noise on embryos with wild-type division rules and timing offset. We found that there exists a region where no cell rearrangements occur and that increasing each type of noise additively increases the rearrangement error rate. Next, we varied the mean timing offset and the timing noise at three values of angular noise. We find that changing the offset between AB and P1 so that P1 divides first leads to a non-lethal rearrangement of ABa and ABp for moderate amounts of timing and angular noise. Finally, we systematically varied the division angles of AB and P1 independently and mapped out the connection between division angles and final cell arrangements. We found that the four final arrangements are partitioned by whether AB's division is below or above 90 degrees and then whether P1's division is below or above 90 degrees.

Our work suggests that embryos may use physical constraints for hierarchical error correction (in this case using a shell, division rules and cell timings) to robustly achieve certain precise arrangements. In the case of *C. elegans*, a coarse constraint on cell arrangements is provided by the egg shell's confining volume and specific aspect ratio. There is only room for a diamond arrangement of four cells[72] which is a sizable reduction from

the full combinatorial space of possible four cell arrangements (6 connected topologies with 38 possible permutations). Within this one diamond topology, there are 6 distinct ways of arranging the cells within this pattern. The proper wildtype arrangement is then robustly selected using division rules and a timing offset between AB and P1 divisions.

Interestingly, the wildtype division rules that have AB divide perpendicular to the AP axis (at 90 degrees for the definition used here) and the P1 division along the AP axis would seem to not be robust to small errors in AB division direction which could reverse ABA and ABp. It is well-known that ABa and ABp are equivalent and that it is the contact with the Delta-expressing P2 that causes ABp's fate to differ from ABa's [48, 49]. The fact that such a division rule would not be robust to small errors is another indication that ABa-ABp misplacement is not on its own detrimental to further development, otherwise a more robust division rule would have been selected for. On the other hand, the wildtype rule is very robust against division angle noise in the P1 division and is as far as possible from 90 degrees (or even 45 degrees which can rarely lead to errors).

Although previous work has mentioned the roles of the shell and division timings for embryo robustness, their simulations have not examined this question in detail. Fickentscher et al (2013)[15] introduced a repulsive particle model that closely matched the trajectories observed in SPIM imaged embryos before gastrulation. They subsequently investigated timing rules inversely related to volume and added asymmetric divisions[16]. [72] adapted the Fickentscher model and added asymmetric adhesion to the model show-

ing that this better matched the arrangements observed when changing the egg shell aspect ratio.

Our work makes several assumptions including that all cell divisions are symmetric, the egg shell is perfectly ellipsoidal, all contact angles between cells are the same, and simplifies the cell-cell interactions to a pair potential that does not take into account higher order effects from other neighbors. Future work could add in the effects of asymmetric divisions and varying adhesion between different cells. Yamamoto and Kimura (2017)[72], for example, finds that the contact angle of P2 is less than for the other 3 cells.

On the whole, our work develops a framework to investigate how early embryos robustly achieve specific cell arrangements using mechanical constraints, cell division timings and timing offsets, and division rules. It also demonstrates the utility of using 3D Voronoi tessellation and adjacency matrices to automatically recognize what arrangements are present in the hundreds of thousands of simulations needed to map the robustness of parameter space which was out of reach of previous simulation frameworks that depended only on cell center distances.

Chapter 4

Concluding Remarks and Future Directions

The correct packings and arrangements of cells in the early embryos of many species are critical for subsequent development to proceed properly. The physical interactions of cells with each other and with the shell or envelope surrounding them strongly constrain what packings are possible and what arrangements will result from division rules and division timings. Using a 3D Voronoi-augmented Langevin simulator, in Chapter 2, we systematically studied what effects varying division rules, division times, and cell-cell adhesion had on unconfined cell packings and on how confinement could override division rules and force only a single packing to be possible. In Chapter 3, we investigated how cells were arranged within a well-defined cellular packing, how robust those arrangements were to timing noise and angular noise and how division rules lead to final cell arrangements.

Overall, we find a hierarchical method of specifying a particular cellular arrangement, first by specifying the packing with a confining shell and then by guiding cells to particular positions within that packing through specific division rules and division timings. For a cluster of 4 cells, there exists, in general, 6 distinct packing topologies with 38 different permuted arrangements of cells distributed among the packing topologies. With strong confinement, we can collapse the 6 packing topologies to just one! If that packing is the diamond (as for *C. elegans*), there are still 6 possible cell arrangements. However, two of those arrangements are not reachable by biologically relevant division rules and the rules necessary to reach the other four are described in Chapter 3. In this way, one can robustly pick one particular arrangement out of 38. The broad framework described by this work provides a set of principles to navigate the large combinatorial space present with even a few cells.

Below, we review the main conclusions of Chapters 2 and 3 and suggest future extensions.

4.1 Conclusions

The goal of Chapter 2 was to identify the ranges of physical parameters that would robustly lead to the different cellular packings observed in the early embryos of diverse species. First, by looking at unconfined clusters, we ruled out that most of the packings could be robustly generated by specific division rules or division timings including the minimal energy tetrahedron. Then, by imposing a repulsive shell, and reducing the inter-

nal shell volume, it was possible to robustly specify a single cellular packing regardless of division rules. The packing could be tuned from the tetrahedron to the diamond to the line by increasing the shell's aspect ratio. Finally, the effect of a sticky shell was studied to determine whether this could lead to a robust square arrangement like that found in echinoderms[19], but although the square arrangement was found, it did not occur more than 40% of the time.

Several extensions to the work in Chapter 2 can be proposed. First, a more systematic exploration of the studied physical parameters could be conducted. Only two contact angles were studied for the case of unconfined arrangements and only one value was used in the subsequent work from the time to reach equilibrium to the arrangements under confinement. When unconfined, contact angles near zero could help stabilize the square against relaxation to the diamond by opening a hole between the four cells. Furthermore, they may allow the T-shaped packing to persist when confined. Also, only two division rules (ordered and random) were investigated. There are many other possible and biologically relevant division rules that could be explored and some may quickly lead to particular packings.

Only random divisions were studied when the clusters were repulsively confined. In the case of the strongly confined shell with an aspect ratio of 2.5, there were two arrangements that persisted for very long times. Could division rules robustly specify one of the packings over the other? Also, only five values of the aspect ratio were simulated. It would be valuable to simulate many more aspect ratio values and determine the precise

values where the equilibrium packing under strong confinement starts to change and the aspect ratio ranges where several metastable packings can coexist.

Real embryo shells are not perfect ellipsoids and early cell divisions are often asymmetric. Simulations could be compared more quantitatively to observed embryo packings if the shells could be specified more precisely and if the relative sizes (and differential adhesions between cells) was taken into account. One regime where properly modelling the shell would lead to improved predictions is the case of embryos with high aspect ratio shells[57] where the shell is better approximated as an elongated cylinder with hemispherical end caps than by an elongated ellipsoid which would cause a strong central restoring force that is not present in the real embryo. Shells are also not always best approximated as perfectly rigid boundaries. In the case of the square sea urchin embryos, observations indicate that cell-cell forces are sufficient to deform the hyaline layer that tightly surrounds the developing embryo[66, 13]. It may be the case that at the four cell stage when the square packing is robustly observed, the previous cell division may have deformed the hyaline layer into an oblate spheroid (pancake) instead of the perfect sphere considered in Chapter 2. This may account for why the square packing was not found to be robust in our simulations, but is robustly observed during sea urchin embryogenesis.

In Chapter 3, the goal was to elucidate the robustness of the wildtype *C. elegans* four cell arrangement to noise in division timing and in the angles of the division axis. The noise values below which the embryo had no errors were found and the errors that occurred at higher noise values were subdivided into sequence errors caused by large

amounts of timing noise and into placement errors where cells ended up in the wrong arrangement due to large amounts of division axis angle noise. Changing the relative offset in division times between AB and P1 only led to the non-lethal ABa-ABp interchange for moderate values of timing and angle noise. Finally, the space of division rules was mapped showing which final arrangements result from particular choices of division angle for the AB and P1 divisions and demonstrating a robust separation between the four arrangements.

Mapping out how division rules map to final arrangements presents a way of deducing if early blastomeres may be initially equivalent like ABa and ABp in *C. elegans*. The wildtype T division rule used by *C. elegans* has the AB division occur 90 degrees from the anterior-posterior axis which according to the division rule flow diagram is exactly between angles that would lead to ABa being anterior ($< 90°$) or posterior ($> 90°$). The fact that the wildtype division rule cannot robustly specify which cell will end up more anterior suggests that this kind of error is not relevant to development. Looking at other embryos and whether their arrangements are robust to the wildtype division rule may suggest which cells are developmentally equivalent even if this has not already been experimentally verified. Conversely, if a division rule is maximally far from causing an arrangement error (like the P1 division perfectly along the AP axis), this may suggest that such an arrangement error would be highly detrimental to subsequent development.

For full generality in specifying division rules, one should not only specify the angle θ from the AP axis, but also the angle ϕ around the axis. In Chapter 3, ϕ was chosen

uniformly at random. When one of the divisions is aligned with the AP axis, any choice of ϕ is degenerate due to the rotational symmetry of the shell. However, when both divisions are not parallel with the AP axis, the relative angle between the two division axes should be taken into account. One can imagine that the arrangements will be very different if both AB and P1 divide at 90 degrees to the AP axis whether they are aligned or anti-aligned. The relative angle between the division axes should be used to subdivide what θ values lead to arrangement errors to better understand the exact mechanism leading to an error.

The simulation used in Chapter 3 can be expanded in a number of ways. First, the wildtype arrangement's robustness to further sources of noise including variations in relative adhesion strength between cells and asymmetries in division could be tested. If such studies revealed a strong sensitivity to one of these parameters, it may indicate why differences in adhesion or cell size occur in real embryos. Next, a model linking cell volume to division time similar to that used by Fickentscher *et al.* (2016)[16] could be added to add a coupling between asymmetric division rules and division timings. While not as precise as shapes found via Surface Evolver in [45], semi-quantitative shape information derived from the 3D Voronoi polytope could be used with a model of division plane positioning to incorporate more biologically plausible division rules. These additions would be aimed at expanding the validity of the simulator beyond the 4-cell regime.

Proper cell positioning and timing become more important for higher numbers of cells. For clusters with four cells, there are 6 different cell topologies with 38 different

cell identity permutations. However, strong shell constraints often lower the number of cell topologies to just one. For higher numbers of cells, the total set of possible topologies and cell positions explodes. Even going up by one cell to five cells leads to 21 different topologies and 728 different cell permutations! Again, the overall shell constraint will lower the number of topologies from 21, but for most shell shapes, it will be possible for several topologies to be present. This means that ensuring proper cell division rules and maintaining low noise in division angles and division timing will be necessary in guiding the embryo to the proper topology and the cells to their proper places within the topology. The shell constraint will be much less able to prevent or correct division angle or timing errors for embryos with more than four cells.

4.2 Future Directions

Several future experiments are suggested by the results of Chapters 2 and 3. One of the most striking predictions of Chapter 2 is that packings other than the tetrahedron can persist for times much longer than the mechanical relaxation time for two cells. This could be tested by removing the shell or external envelope of a fertilized egg, allowing it to develop to the four cell stage and then treating it with a cell-cycle arresting compound to prevent further divisions. Then, the time to reach the tetrahedron could be recorded. This time could be compared to the mechanical relaxation time between two cells which could be determined by pipette[35] or dual pipette aspiration[9].

Our predictions for the effect of decreasing confining shell volume on the observed

cell packings could be tested by placing fertilized eggs (with their shells or envelopes removed) into elliptically shaped wells of different volumes and recording the resulting packings. These wells could be made of PDMS like in those used to study the effect of cell shape on division plane positioning[40]. While it would be difficult to approximate the full 3D ellipsoid shape, making an ellipsoidal prism would be straightforward and could be compared to new simulations.

As mentioned above, our study of robustness indicates that certain division angles (near 90°) are sensitive to small amounts of angular noise which can lead to changes in cell placement. We found that for *C. elegans*, the AB division was sensitive to noise, but that the ABa and ABp cells were developmentally equivalent and their fate specification was set by Notch/Delta signalling through contact with P1[49]. By cataloguing the wildtype division rules of other nematode species (and other species more generally), we could use our robustness simulation to determine if a species' division rule was sensitive to noise which could let us quickly identify possible developmentally equivalent blastomeres in early development. The equivalence of these cells could then be tested by manually manipulating the position of the cells or by investigating cell genetic expression with single cell transcriptomics.

Finally, an apparatus for generating strong temperature gradients in *C. elegans* can be used to experimentally alter the division timing offset between AB and P1[63]. The overall timing of embryonic divisions has been found to predictably vary with temperature. By subjecting parts of the embryo to different temperatures (with up to a 7°C

difference between the two ends of the embryo), it was possible to change the timing difference between P1 and AB and even to reverse the division order. While none of the embryos where P1 divided before AB hatched, they did produce "worm-like" organisms suggesting that proper timing was necessary for subsequent fate specification. Data from these experiments could be quantitatively compared to the predictions in Chapter 3 by checking the frequency of AB shifts and the frequency of other types of errors.

Several future applications and extensions of the simulator are also worth discussing. Due to its computational tractability, the simulator described above can easily be extended to the large N limit to study the properties of active foams and models of tissues. Investigations into the mechanical properties of tissues undergoing morphogenesis suggest that some tissues are undergoing a fluid-to-solid transition, reminiscent of a jamming or glass transition[27, 33, 56]. In Mongera *et al.* (2018)[42], the transition seemed to be controlled by changes in the volume fraction intracellular spaces in the MPZ compared with the PSM. Cell force fluctuations were also observed and increases in fluctuations was associated with an increased number of observed T1 transitions which are one of the main ways stresses can be relaxed in these materials. It would be useful to have a computational platform to investigate the effects of changes in cell-cell adhesion and the strength of cell-fluctuations on the collective material properties of the tissue as a whole. Previous work which used a self-propelled Voronoi model like Bi *et al.* (2016)[8] and Merkel and Manning (2017)[39] do not allow spaces to open between cells since the Voronoi partition used extends through all of space. The simulator used in this work,

however, bounds the maximum size of the Voronoi polytopes allowing for spaces to open up in simulated tissue. Such a platform could be used to map out the phase diagram of jamming matter subject to active fluctuations including changes in tissue volume fraction which cannot be studied with previous Voronoi models.

To more fully predict and understand cell packings and arrangements later in embryo development, it will be necessary to keep track of internal cell states and to have feedback between cell states and cell physical parameters and division rules and timings. Cell-cell signalling can lead to asymmetric divisions, repositioning of the division plane, changes in division timing, and changes in cell-cell adhesion strength. The 3D Voronoi polytopes give an approximate estimate of the surface area of cell-cell contacts which could be used to incorporate biologically plausible surface-area dependent cell-cell signalling and could be used to modulate the interaction potential between two cells as currently any amount of contact will lead to the same force which only depends on cell center distance. Chemical differential equations that describe stochastic gene expression due to cell signalling could be incorporated into the simulation closing the loop between physical dynamics and internal state dynamics. To study the next stages of embryogenesis, it will be necessary to incorporate such iterative loops into simulation.

Bibliography

[1] D L Adelson and T Humphreys. Sea urchin morphogenesis and cell-hyalin adhesion are perturbed by a monoclonal antibody specific for hyalin. *Development (Cambridge, England)*, 104(3):391–402, November 1988.

[2] Natalie Arkus, Vinothan N Manoharan, and Michael P Brenner. Minimal Energy Clusters of Hard Spheres with Short Range Attractions. *Physical Review Letters*, 103(11):118303–4, September 2009.

[3] Natalie Arkus, Vinothan N Manoharan, and Michael P Brenner. Deriving Finite Sphere Packings. *SIAM Journal on Discrete Mathematics*, 25(4):1860–1901, January 2011.

[4] S Artavanis-Tsakonas, M D Rand, and R J Lake. Notch signaling: cell fate control and signal integration in development. *Science*, 284(5415):770–776, April 1999.

[5] Zhirong Bao, Zhongying Zhao, Thomas J Boyle, John I Murray, and Robert H Waterston. Control of cell cycle timing during C. elegans embryogenesis. *Developmental biology*, 318(1):65–72, June 2008.

[6] Vanessa Barone and Carl-Philipp Heisenberg. Cell adhesion in embryo morphogenesis. *Current Opinion in Cell Biology*, 24(1):148–153, February 2012.

[7] Eyal Ben-David, Alejandro Burga, and Leonid Kruglyak. A maternal-effect selfish genetic element in Caenorhabditis elegans. *Science*, 356(6342):1051–+, 2017.

[8] Dapeng Bi, Xingbo Yang, M Cristina Marchetti, and M Lisa Manning. Motility-Driven Glass and Jamming Transitions in Biological Tissues. *Physical Review X*, 6(2):021011–13, April 2016.

[9] Maté Biro and Jean-Léon Maître. Dual pipette aspiration: a unique tool for studying intercellular adhesion. *Methods in cell biology*, 125:255–267, 2015.

[10] Kenneth A. Brakke. The surface evolver. *Experiment. Math.*, 1(2):141–165, 1992.

[11] Michael Brauchle, Karine Baumer, and Pierre Gönczy. Differential activation of the DNA replication checkpoint contributes to asynchrony of cell division in C. elegans embryos. *Current Biology*, 13(10):819–827, May 2003.

[12] K M Cadigan and R Nusse. Wnt signaling: a common theme in animal development. *Genes & Development*, 11(24):3286–3305, December 1997.

[13] E Citkowitz. The hyaline layer: its isolation and role in echinoderm development. *Developmental biology*, 24(3):348–362, March 1971.

[14] U Deppe, E Schierenberg, T Cole, C Krieg, D Schmitt, B Yoder, and G von Ehrenstein. Cell lineages of the embryo of the nematode Caenorhabditis elegans. *Proceedings of the National Academy of Sciences*, 75(1):376–380, January 1978.

[15] Rolf Fickentscher, Philipp Struntz, and Matthias Weiss. Mechanical Cues in the Early Embryogenesis of Caenorhabditis elegans. *Biophysj*, 105(8):1805–1811, October 2013.

[16] Rolf Fickentscher, Philipp Struntz, and Matthias Weiss. Setting the Clock for Fail-Safe Early Embryogenesis. *Physical Review Letters*, 117(18):188101, October 2016.

[17] Rolf Fickentscher and Matthias Weiss. Physical determinants of asymmetric cell divisions in the early development of Caenorhabditis elegans. *Scientific Reports*, 7(1):9369, August 2017.

[18] R L Gardner. Experimental analysis of second cleavage in the mouse. *Human Reproduction*, 17(12):3178–3189, December 2002.

[19] Scott F. Gilbert and Michael J. F. Barresi. *Developmental Biology*. Sinauer Associates, Inc, 11 edition, 2016.

[20] Taryn E Gillies and Clemens Cabernard. Cell Division Orientation in Animals Review. *Current Biology*, 21(15):R599–R609, August 2011.

[21] B Goldstein. On the evolution of early development in the Nematoda. *Philosophical transactions of the Royal Society of London. Series B, Biological sciences*, 356(1414):1521–1531, October 2001.

[22] Stephan W Grill and Anthony A Hyman. Spindle Positioning by Cortical Pulling Forces. *Developmental Cell*, 8(4):461–465, April 2005.

[23] B J Gulyas. A reexamination of cleavage patterns in eutherian mammalian eggs: rotation of blastomere pairs during second cleavage in the rabbit. *The Journal of experimental zoology*, 193(2):235–248, August 1975.

[24] Mark A Hill. Sea Urchin Development. https://embryology.med.unsw.edu.au/embryology/index.php/Sea_Urchin_Development. Accessed: 2020-01-15.

[25] M R Hoare and J McInnes. Statistical mechanics and morphology of very small atomic clusters. *Faraday Discussions of the Chemical Society*, 61:12–13, 1976.

[26] Miranda Holmes-Cerfon, Steven J Gortler, and Michael P Brenner. A geometrical approach to computing free-energy landscapes from short-ranged potentials. *Proceedings of the National Academy of Sciences*, 110(1):E5–E14, 2013.

[27] Atsushi Ikeda, Ludovic Berthier, and Peter Sollich. Unified study of glass and jamming rheology in soft particle systems. *Physical Review Letters*, 109(1):018301–5, July 2012.

[28] Peter E Kloeden and Eckhard Platen. *Numerical Solution of Stochastic Differential Equations*. Springer Science & Business Media, Berlin, Heidelberg, April 2013.

[29] Rose L. and Gnczy P. *WormBook*, chapter Asymmetric cell division and axis formation in the embryo. WormBook, 10 2005. 10.1895/wormbook.1.30.1.

[30] Rose L. and Gnczy P. *WormBook*, chapter Polarity establishment, asymmetric division and segregation of fate determinants in early C. elegans embryos. WormBook, 12 2014. 10.1895/wormbook.1.30.2.

[31] R H Leary. Global optima of Lennard-Jones clusters. *Journal of Global Optimization*, 11(1):35–53, July 1997.

[32] Thomas Lecuit, Pierre-François Lenne, and Edwin Munro. Force Generation, Transmission, and Integration during Cell and Tissue Morphogenesis. *Annual Review of Cell and Developmental Biology*, 27(1):157–184, November 2011.

[33] Andrea J Liu and Sidney R Nagel. The Jamming Transition and the Marginally Jammed Solid. *Annual Review of Condensed Matter Physics*, 1(1):347–369, August 2010.

[34] Jean-Leon Maitre, Hélène Berthoumieux, Simon Frederik Gabriel Krens, Guillaume Salbreux, Frank Jülicher, Ewa Paluch, and Carl-Philipp Heisenberg. Adhesion functions in cell sorting by mechanically coupling the cortices of adhering cells. *Science*, 338(6104):253–256, October 2012.

[35] Jean-Leon Maitre, Ritsuya Niwayama, Herve Turlier, François Nédélec, and Takashi Hiiragi. Pulsatile cell-autonomous contractility drives compaction in the mouse embryo. *Nature Cell Biology*, 17(7):849–855, July 2015.

[36] V N Manoharan. Dense Packing and Symmetry in Small Clusters of Microspheres. *Science*, 301(5632):483–487, July 2003.

[37] David R McClay. Evolutionary crossroads in developmental biology: sea urchins. *Development*, 138(13):2639–2648, 2011.

[38] G Meng, N Arkus, M P Brenner, and V N Manoharan. The Free-Energy Landscape of Clusters of Attractive Hard Spheres. *Science*, 327(5965):560–563, January 2010.

[39] Matthias Merkel and Lisa Manning. A geometrically controlled rigidity transition in a model for confluent 3D tissues. *arXiv.org*, June 2017.

[40] Nicolas Minc, David Burgess, and Fred Chang. Influence of Cell Geometry on Division-Plane Positioning. *Cell*, 144(3):414–426, February 2011.

[41] Nicolas Minc and Matthieu Piel. Predicting division plane position and orientation. *Trends in Cell Biology*, 22(4):193–200, April 2012.

[42] Alessandro Mongera, Payam Rowghanian, Hannah J Gustafson, Elijah Shelton, David A Kealhofer, Emmet K Carn, Friedhelm Serwane, Adam A Lucio, James Giammona, and Otger Campàs. A fluid-to-solid jamming transition underlies vertebrate body axis elongation. *Nature*, 561(7723):401–405, September 2018.

[43] J A Northby. Structure and binding of Lennard-Jones clusters: $13 \leq N \leq 147$. *The Journal of Chemical Physics*, 87(10):6166–13, 1987.

[44] Ewa Paluch and Carl-Philipp Heisenberg. Biology and Physics of Cell Shape Changes Review in Development. *Current Biology*, 19(17):R790–R799, September 2009.

[45] Anaëlle Pierre, Jérémy Sallé, Martin Wühr, and Nicolas Minc. Generic Theoretical Models to Predict Division Patterns of Cleaving Embryos. *Developmental Cell*, 39(6):667–682, December 2016.

[46] K Piotrowska-Nitsche and M Zernicka-Goetz. Spatial arrangement of individual 4-cell stage blastomeres and the order in which they are generated correlate with blastocyst pattern in the mouse embryo. *Mechanisms of Development*, 122(4):487–500, April 2005.

[47] Christian Pohl. Left-right patterning in the C. elegans embryo: Unique mechanisms and common principles. *Communicative & integrative biology*, 4(1):34–40, January 2011.

[48] J R PRIESS and J N Thomson. Cellular Interactions in Early C-Elegans Embryos. *Cell*, 48(2):241–250, 1987.

[49] James R. Priess. *WormBook*, chapter Notch signaling in the C. elegans embryo. WormBook, 6 2005. 10.1895/wormbook.1.4.1.

[50] E M Purcell. Life at low Reynolds number. *American Journal of Physics*, 45(1):3–11, January 1977.

[51] Julia L Richards, Amanda L Zacharias, Travis Walton, Joshua T Burdick, and John Isaac Murray. A quantitative model of normal Caenorhabditis elegans embryogenesis and its disruption after stress. *Developmental biology*, 374(1):12–23, February 2013.

[52] Chris H Rycroft. VORO++: a three-dimensional voronoi cell library in C++. *Chaos (Woodbury, N.Y.)*, 19(4):041111, December 2009.

[53] Guillaume Salbreux, Guillaume Charras, and Ewa Paluch. Actin cortex mechanics and cellular morphogenesis. *Trends in Cell Biology*, 22(10):536–545, October 2012.

[54] einhard schierenberg and Bernd Junkersdorf. The role of eggshell and underlying vitelline membrane for normal pattern formation in the early C. elegans embryo. *Roux's archives of developmental biology : the official organ of the EDBO*, 202(1):10–16, December 1992.

[55] R Schnabel, H Hutter, D Moerman, and H Schnabel. Assessing normal embryogenesis in Caenorhabditis elegans using a 4D microscope: Variability of development and regional specification. *Developmental biology*, 184(2):234–265, 1997.

[56] E M Schotz, M Lanio, J A Talbot, and M L Manning. Glassy dynamics in three-dimensional embryonic tissues. *Journal of The Royal Society Interface*, 10(89):20130726–20130726, September 2013.

[57] Jens Schulze and Einhard Schierenberg. Evolution of embryonic development in nematodes. *Evodevo*, 2(1):18, September 2011.

[58] Friedhelm Serwane, Alessandro Mongera, Payam Rowghanian, David A Kealhofer, Adam A Lucio, Zachary M Hockenbery, and Otger Campàs. In vivo quantification of spatially varying mechanical properties in developing tissues. *Nature methods*, 14(2):181–186, February 2017.

[59] Yuichiro Shibazaki, Miho Shimizu, and Reiko Kuroda. Body Handedness Is Directed by Genetically Determined Cytoskeletal Dynamics in the Early Embryo. *Current Biology*, 14(16):1462–1467, August 2004.

[60] NJA Sloane, R H HARDIN, TDS DUFF, and J H CONWAY. Minimal-Energy Clusters of Hard-Spheres. *Discrete & Computational Geometry*, 14(3):237–259, October 1995.

[61] Martin P Stewart, Jonne Helenius, Yusuke Toyoda, Subramanian P Ramanathan, Daniel J Muller, and Anthony A Hyman. Hydrostatic pressure and the actomyosin cortex drive mitotic cell rounding. *Nature*, 469(7329):226–230, 2011.

[62] J E Sulston, E Schierenberg, J G White, and J N Thomson. The Embryonic-Cell Lineage of the Nematode Caenorhabditis-Elegans. *Developmental biology*, 100(1):64–119, 1983.

[63] E S Terry. *A Microfluidic Temperature Gradient Device and Its Application to Uncovering Temporal Systems of Robustness in the Developing Embryo of the Nematode C. elegans*. Ph.d. thesis, UC Santa Barbara, December 2017.

[64] D. Wales, R. Saykally, A. Zewail, and D. King. *Energy Landscapes: Applications to Clusters, Biomolecules and Glasses*. Cambridge Molecular Science. Cambridge University Press, 2003.

[65] S Ward and J Miwa. Characterization of temperature-sensitive, fertilization-defective mutants of the nematode caenorhabditis elegans. *Genetics*, 88(2):285–303, February 1978.

[66] G M Wessel, L Berg, D L Adelson, G Cannon, and D R MCCLAY. A molecular analysis of hyalin–a substrate for cell adhesion in the hyaline layer of the sea urchin embryo. *Developmental biology*, 193(2):115–126, January 1998.

[67] H A Wilkinson, K Fitzgerald, and I Greenwald. Reciprocal changes in expression of the receptor lin-12 and its ligand lag-2 prior to commitment in a C. elegans cell fate decision. *Cell*, 79(7):1187–1198, December 1994.

[68] A Wodarz and R Nusse. Mechanisms of Wnt signaling in development. *Annual Review of Cell and Developmental Biology*, 14(1):59–88, 1998.

[69] Inc. Wolfram Research. Mathematica, version 11.3, 2018. Champaign, IL.

[70] W B WOOD, D Bergmann, and A Florance. Maternal effect of low temperature on handedness determination in C. elegans embryos. *Developmental genetics*, 19(3):222–230, 1996.

[71] W B WOOD, R HECHT, S CARR, R VANDERSLICE, N WOLF, and D HIRSH. Parental Effects and Phenotypic Characterization of Mutations That Affect Early Development in Caenorhabditis-Elegans. *Developmental biology*, 74(2):446–469, 1980.

[72] Kazunori Yamamoto and Akatsuki Kimura. An asymmetric attraction model for the diversity and robustness of cell arrangement in nematodes. *Development*, 144(23):4437–4449, December 2017.